57

00-1616-14

A Facsimile Report

1

Reproduced by
UNITED STATES
ATOMIC ENERGY COMMISSION
Division of Technical Information
P.O. Box 62 Oak Ridge, Tennessee 37830

SQT.64272R

United States Atomic Energy Commission

Technical Report No. COO-AT(11-1)-1616-14

Studies of Nickelous and Cobaltous Oxide and Effects of n-Type and p-Type Dopants

William Rives Helms*

Physics Department, Purdue University

Lafayette, Indiana

*This report is based on a thesis submitted in partial fulfillment of the requirements of the degree of Doctor of Philosophy at Purdue University.

ACKNOWLEDGMENTS

I would like to express my appreciation to Professor James G. Mullen for originally suggesting the topic reported in this thesis and for providing encouragement and professional guidance throughout the course of this research. I would also like to acknowledge helpful discussions with my fellow graduate students. I would like to thank Professor H. J. Yearian for the generous use of his x-ray diffractometer. This work was supported in part by the United States Atomic Energy Commission, the General Electric Company, and the National Aeronautics and Space Administration.

TABLE OF CONTENTS

TABLE OF CONTENTS (Contd)

LIST OF TABLES

LIST OF FIGURES

Figure — Page

LIST OF SYMBOLS

Symbol	Name
CoO, NiO	Generic terms denoting cobaltous oxide or nickelous oxide
CoO(I), NiO(I)	High temperature forms of CoO or NiO, having perfect translational symmetry and revealing only Fe^{2+} in the Mössbauer resonance resulting from the decay of Co^{57}
CoO(I,II), NiO(I,II)	High temperature forms of CoO or NiO indicating both Fe^{2+} and Fe^{3+} in the Mössbauer resonance
CoO(1% Li), NiO(1% Li)	High temperature preparations of CoO or NiO with a 1% Li^{1+} doping
CoO(II), NiO(II)	Low temperature forms of CoO or NiO which are pure and nominally stoichiometric, and give only Fe^{3+} in the Mössbauer resonance
CoO*, NiO*	Non-stoichiometric CoO or NiO prepared at low temperature containing impurities from the nitrate or carbonate used as starting material
CoO · nO	CoO(II) which has been allowed to pickup excess oxygen from the initial stoichiometric composition, but which has the basic x-ray pattern of cobaltous oxide
MO	Mullen and Ok
v	Relative velocity between source and absorber in a Mössbauer experiment, taken as positive when the absorber moves toward the source
c	Speed of light
E_γ	Nuclear transition energy
A(v)	Fractional Mössbauer effect as a function of velocity

Symbol	Name
S	Area under Mössbauer absorption line
Γ	Full width at half maximum of Mössbauer absorption line
v_o	Velocity of the center of the Mössbauer absorption line
$\mathring{A}$	Angstrom
R	Recoil energy
T	Absolute temperature
k	Boltzmann constant
T_N	Néel temperature
θ_p	Paramagnetic Néel temperature
τ	Superparamagnetic relaxation time
τ_L	Larmor precession time
f_o	Frequency factor
K	Anisotrophy energy per unit volume
V	Volume of particle
θ	Debye temperature
θ_m	Mössbauer characteristic temperature
u	Displacement of atom in the direction of gamma ray emission
$\vec{\kappa}$	Gamma ray wave vector
$\|n\rangle$	Eigenstate of the lattice
$\vec{r}$	Displacement vector of nuclear motion
f	Recoil-free fraction
$\mathcal{H}_g$	Hamiltonian of ground state of Fe^{57}

Symbol	Name
$\mathcal{H}_e$	Hamiltonian of first excited state of Fe^{57}
g_0	Nuclear gyromagnetic ratio of the ground state of Fe^{57}
g_1	Nuclear gyromagnetic ratio of the first excited state of Fe^{57}
μ_N	Nuclear Bohr magneton
$\vec{I}$	Nuclear spin
$\vec{H}$	Magnetic field at nucleus
E_m	Eigenvalue of magnetic hyperfine interaction
m	Magnetic quantum number

ABSTRACT

Helms, William Rives. Ph.D., Purdue University, August 1970. Studies of Nickelous and Cobaltous Oxide and Effects of n-type and p-type Dopants. Major Professor: James G. Mullen.

Mössbauer, chemical, and x-ray studies establish that the low temperature preparations of cobaltous and nickelous oxide have significant structural differences from high temperature preparations. The data cannot be explained by electronic effects alone, and ion size effects have been ruled out. The structural model most compatible with experiment involves a combination of Schottky vacancies and porosity. The low temperature stoichiometric preparations, CoO(II) and NiO(II), may be viewed as a sponge-like structure, with a large concentration of dispersed anion and cation vacancies. Schottky defects appear to be responsible for most of the observed differences between high and low temperature forms. The data are consistent with the charge stabilization of the Fe^{3+} ion by electron trapping at oxygen vacancies. Our results do not indicate that stoichiometric variations are the main cause of differences in the properties of the high and low temperature forms. Nominally stoichiometric and pure NiO(II) can be prepared at low temperature, analogous to an earlier preparation of CoO(II). NiO(II) and CoO(II) represent a saturated non-equilibrium density of Schottky defects and porosity. Attempts to increase this defect density result in impure and non-stoichiometric materials, denoted as NiO* and CoO*. The Mössbauer patterns of NiO(II) and

CoO(II) exhibit only the Fe^{3+} resonance. The density of NiO(II) is $6.0 \pm .2$ g/cm^3, or about 12% below the value expected from x-ray data. The Néel temperature, T_N, is measured to be $515 \pm 5^\circ$K. T_N for a high temperature sample is measured to be $525 \pm 1^\circ$K. The temperature dependence of the magnetic hyperfine field for NiO(II) follows the Brillouin function for S = 5/2, approximately. NiO(II) shows only the expected x-ray diffraction peaks, although broadened, and it has a Mössbauer characteristic temperature, θ_m, of $350 \pm 10^\circ$K. The physical adsorption of Ar and Ne gases by CoO(II) and NiO(II) gives an estimate of particle size of order 100 Å, in accord with x-ray line broadening. The pickup of oxygen by CoO(II) is in sharp contrast to NiO(II), which is inert in oxygen. An explanation for the magnitude of the oxygen pickup of CoO(II) (in excess of 60% of the stoichiometric value) has not been found, although we show that the process cannot be a physical adsorption. The application of an external magnetic field to NiO* gives evidence for superparamagnetism resulting from small particle size, which is not found for form II samples. Experiments in which NiO and CoO are doped with Li, Cr, and Ga have shown that significant changes in the ratio Fe^{2+}/Fe^{3+} are obtained. Li doping enhances the Fe^{3+} resonance, while Cr and Ga enhance the Fe^{2+} resonance. The qualitative effects of the dopants are explained using a band model for these semiconducting oxides. The value of θ_m for the Fe^{3+} resonance induced by Li in high temperature preparations is $410 \pm 10^\circ$K for CoO(1% Li) and $420 \pm 10^\circ$K for NiO(1% Li). These results, compared with the earlier value of θ_m for CoO(II), which has been determined with improved accuracy for this study, demonstrate the structural

differences between high and low temperature preparations. By measuring changes in the Néel temperature in high temperature lithium doped samples, and in CoO(II) and NiO(II), we are able to estimate the relative partitioning of Schottky defects as compared with porosity. The results indicate that about 1/4 of the 25% density lowering in CoO(II) is due to Schottky defects and 3/4 is due to porosity. In NiO(II) it is estimated that about 1/6 of the 12% density lowering is due to Schottky defects and 5/6 is due to porosity. The ratio of the fractional reductions in θ_m for CoO(II) and NiO(II) is the same as the ratio of the estimated fractional amounts of Schottky defects in CoO(II) and NiO(II), which gives added support to the above analysis based on changes in the Néel temperature. The doping experiments indicate that the unusual increase of the Fe^{3+} resonance with temperature, in forms which contain both Fe^{2+} and Fe^{3+}, is a consequence of the semiconducting properties of these materials and does not require a diffusion of cation or anion vacancies, as had been speculated earlier. Our results indicate that the doping technique should be a useful tool in studying the semiconducting properties of the transition metal oxides. We have found a very useful application for cobaltous oxide, doped with lithium, in the preparation of compact, single line sources, which have very narrow linewidths and exceptionally large recoil-free fractions.

I. INTRODUCTION

In 1958 Rudolf Mössbauer[1] discovered that nuclei bound in a crystalline lattice can emit and absorb gamma rays, which display the natural linewidth and possess the full transition energy, with no recoil energy transferred to lattice vibrations. The importance of this condition is that the recoil energy of a nucleus (required by momentum conservation) emitting a gamma ray is several orders of magnitude greater than the minimum linewidth of the gamma ray. The recoil energy causes absorption and emission lines to be shifted so that no overlap or resonance can occur. Previous to Mössbauer's work various methods to compensate for the recoil energy loss had been tried. These involved doppler shifting the emitted gamma rays with a high speed rotor, doppler broadening the gamma rays by thermal motion, or using a preceeding nuclear event to impart a momentum to the emitting nucleus. Mössbauer showed, however, with the aid of Lamb's theory of resonant neutron scattering, that there is a finite probability that a nucleus will emit or absorb a gamma ray without a change in the phonon states of the crystal with the recoil momentum being carried away by the entire crystal and not the individual nucleus. In this case the loss of energy by the gamma ray due to the recoil process is negligible, and the gamma ray will also have the minimum width determined by the uncertainty principle from the half-life of the excited state of the nucleus. In the case of Fe^{57}, the most commonly used Mössbauer

isotope, the recoil energy carried away by the nucleus from the 14.4 keV gamma ray would be about 10^{-3} eV if the nucleus were assumed to recoil. But the energy characteristic of lattice vibrations is larger (typically of the order of 10^{-2} to 10^{-1} eV). Since the lattice is a quantized system it cannot be excited in an arbitrary fashion, and therefore there is a finite probability of zero-phonon emission. For the 14.4 keV transition of Fe^{57} the zero-phonon gamma ray will have a width of order 10^{-8} eV, so that its energy is defined to 1 part in 10^{12}.

In a typical Mössbauer experiment one measures the transmission of gamma rays from a source through a resonant absorber. By imparting a relative velocity v between source and absorber, the energy spectrum of the gamma rays from the source can be doppler shifted by an amount $\frac{v}{c}E_\gamma$, where E_γ is the nuclear transition energy and c is the velocity of light. The counting rate at the detector drops whenever the relative doppler velocity shifts the energy of a gamma ray emitted by the source into coincidence with an absorption energy of the absorber. The data are usually put into the form of a plot of percent absorption versus velocity in mm/sec. An energy spectrum of the source can thus be obtained. This new type of spectroscopy is one of the primary tools used to study cobaltous and nickelous oxide in this thesis.

An important property of the Mössbauer effect in Fe^{57} is that the gamma ray linewidth is smaller than the characteristic energy splittings of nuclear levels in crystalline fields, and therefore Mössbauer spectroscopy permits a direct observation of these interactions. Because the nucleus possesses a magnetic dipole moment the nuclear levels will be split if a magnetic field is present at the nuclear

site. In the case of Fe^{57} the magnetic hyperfine interaction splits the excited state and the ground state such that there are six allowed transitions, and the Mössbauer pattern will have six lines. The charge distribution of the nucleus will interact with the distribution of external charge. The lowest order interaction is the monopole interaction between the nucleus and the electron density at the nucleus. This interaction produces a shift in the centroid of the Mössbauer pattern, and this isomer shift can be correlated with the valence of the ion because the total electron density at the nucleus will depend upon the valence state. In the case of Fe^{57}, for example, the isomer shift can be used to clearly differentiate between the Fe^{2+} and Fe^{3+} ions, even without an explicit determination of the nuclear splittings[2]. The valence state of the ion may also be correlated with the magnitude of the magnetic field at the nuclear site to further confirm the charge state of the Mössbauer ion. The second non-vanishing term of the electrostatic interaction of the nucleus with its surrounding charge is the quadrupole interaction. For Fe^{57}, an electric field gradient at the nucleus interacts with the quadrupole moment of the excited state such that there are two allowed transitions. For an Fe^{57} nucleus in a combined magnetic field and electric field gradient, there will be in general eight allowed transitions.

The area under the Mössbauer curve is proportional to the recoil-free fraction for emission and is a measure of the binding of the ion in its lattice site. The stiffer the lattice the greater the probability that an emitted gamma ray will be a zero-phonon or Mössbauer event. The theory of this effect will be discussed in detail in Section II-A,

and it will be applied in discussing our observations.

Since Wertheim's[3] original work on CoO in 1961 much interest has been shown in the Mössbauer spectra of Fe^{57} doped in the transition metal oxides CoO and NiO. The initial interest centered on the observation that the charge state of the Fe^{57} was found to be not only the expected 2+, but also 3+. It was found by different groups[4-14] that depending upon the method of sample preparation, various ratios of the 2+ to 3+ resonance were observed, with lower temperatures of preparation generally giving more Fe^{3+}. The first explanation for the appearance of the Fe^{3+} resonance was due to Wertheim. He interpreted the Fe^{3+} resonance in terms of an Auger electron process, which has sometimes been referred to as an Auger aftereffect. Fig. 1 shows the decay scheme of Co^{57}, which decays via electron capture to Fe^{57}. The Fe^{57} nucleus is initially in an excited state and has the electronic structure of Co^{57}, with an inner electron missing. The resulting hole, which is generally a missing K-electron, is filled by an outer electron with the emission of an x-ray, or alternatively the excitation energy is transmitted to an outer electron referred to as an Auger electron. Each time an Auger electron is emitted, the charge state of the Fe^{57} ion is increased by one. Following this buildup to a high charge state, the highly charged ion will capture electrons until electronic equilibrium is reached. One critical parameter in this process is the time required to reach electronic equilibrium following the Auger cascade. If this time is of the order of or greater than the 10^{-7} second half-life of the 14.4 keV gamma ray used in the Mössbauer measurement, then the higher charged states, caused by the Auger

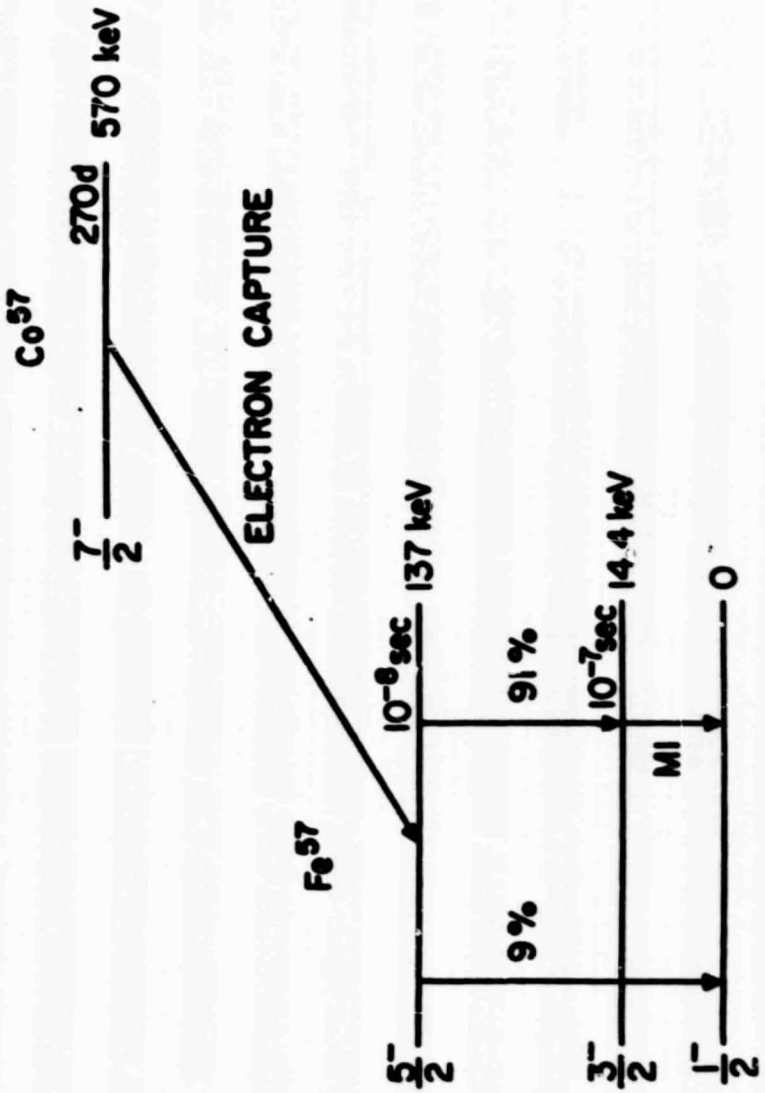

Figure 1. Decay scheme of Co^{57}.

process, will be detected. In metals this return to electronic equilibrium takes place in a time very short compared to the 10^{-7} second half-life of the 14.4 keV gamma ray because of the abundance of conduction electrons. In a dielectric material such as CoO it was not known initially whether this process of capturing electrons would be completed before the Mössbauer observation. Recently Mullen and Ok[6], hereafter referred to as MO, proposed that the stabilization of Fe^{3+} in hydrated salts is due to the radiolysis of water by Auger electrons, and this point has been amplified by Wertheim.[15] This Auger related mechanism, of course, would not apply to anhydrous salts. Bhide and Shenoy[4-5] found similar results in NiO and CoO. They also proposed that the equilibrium fraction of the Fe^{3+} resonance was connected with the semiconducting properties of these oxides. In 1966, two groups simultaneously proved that an Auger aftereffect was not responsible for the Fe^{3+} resonance in these oxides. Triftshauser and Craig[7-8] used delayed coincidence techniques to show that no time effects were observed which could not be attributed to the delayed coincidence technique itself. That is, the return to electronic equilibrium following the Auger process was already completed on the time scale of the Mössbauer observation. They proposed that the appearance of the Fe^{3+} resonance was a result of the deviation of the samples from ideal stoichiometry, caused by a small amount of cation vacancies. MO[6,11] also found no evidence for Auger aftereffects in their studies of CoO and the hydrates of $CoCl_2$. MO isolated two forms of nominally stoichiometric CoO, which showed remarkably different physical properties and were referred to as CoO(I) and CoO(II). CoO(I)

prepared at 1000°C had ideal stoichiometry and density, and showed only the Fe^{2+} Mössbauer line. CoO(II) prepared at 300°C had nominal stoichiometry, but a density about 25% below the theoretical value indicated from the lattice parameter and crystal structure. It was assumed that the 25% reduction in density could be accounted for by point vacancies of Co and O. CoO(II) showed only the Fe^{3+} resonance, and its x-ray diffraction peaks were broader than the ideal high temperature preparation. It was found that the Mössbauer characteristic temperature for the Fe^{3+} resonance was about half that of the Fe^{2+} resonance, and CoO(II) was observed to pickup about 60% excess oxygen when exposed to air. A sample showing both Fe^{2+} and Fe^{3+} resonances was assumed to be a simple mixture of CoO(I) and CoO(II) below a certain temperature and was designated as CoO(I,II). The work of MO represented the first attempt to compare Mössbauer data with other physical and chemical measurements carried out directly on the same samples.

Ando and Kundig[9], along with Schroeer and Triftshauser[12], have explained the differences between the high and low temperature preparations of these oxides as due to particle size effects. Following this approach Schroeer and Triftshauser postulated that CoO(II) consisted of microcrystals of average diameter 50-100 Å. For example, they postulated that the packing of spheres could result in a density lowering if it were assumed that the liquid used in the density measurement could not get into spaces between the particles. The dramatic oxygen pickup of CoO(II) would be due to oxygen settling into defect lattice sites at the surface of the microcrystals, and the Fe^{3+}

resonance was caused by a cation vacancy excess which increased as the microcrystal size decreased. Schroeer and Triftshauser attempted to explain the lower Mössbauer characteristic temperature for CoO(II) as resulting from modifications in the lattice vibrational spectrum due to surface effects and lattice spacing changes. Ando and Kundig[9] used the silica gel technique for restricting particle size, and they found that a sample of NiO prepared at 500°C of average particle size 100 Å showed only the Fe^{3+} resonance. They also supported the view that stoichiometric imbalances caused by the small particle size were responsible for the Fe^{3+} resonance. It was quickly pointed out[13], however, that there were serious difficulties with the quantitative arguments of Schroeer and Triftshauser.

We will show that the data on the oxides can best be explained as a synthesis of several earlier ideas.[14] There is converging agreement toward a model involving both point vacancies and porosity, i.e., the low temperature forms of CoO and NiO contain microscopic or point vacancies (both cation and anion) and holes or pores resulting from sintered microcrystals. Our discussion will assume that there are significant structural differences in the low and high temperature preparations, and we will attempt to correlate our observations with this structural model.

The present thesis will deal mainly with the low temperature preparations of CoO and NiO, whose structure has been a subject of recent controversy[4-14]. MO[11] have carefully studied the high temperature preparations of CoO, and Siegwarth[10] has studied the high temperature preparations of NiO. We will use our earlier notation, i.e.,

CoO(I) and NiO(I) will designate high temperature preparations, showing only the Fe^{2+} resonance, and CoO(II) and NiO(II) will designate pure and nominally stoichiometric low temperature preparations, exhibiting only the Fe^{3+} resonance. CoO(I,II) and NiO(I,II) will denote samples showing both Fe^{2+} and Fe^{3+} resonance. The original basis of this notation is the radical empirical differences found for the high and low temperature preparations. Although it was first thought that CoO(II) might be a different phase than CoO(I), subsequent evidence has not supported this view. There is a conceptual basis, however, for differentiating forms I and II as follows: CoO(II) and NiO(II) appear to represent a saturated non-equilibrium density of Schottky defects in these oxides, accompanied by significant porosity, in contrast to the nearly perfect translational symmetry of CoO(I) or NiO(I). Attempts to increase the Schottky defect density beyond the values indicated for CoO(II) or NiO(II), from either carbonate or nitrate preparations, did not yield pure stoichiometric oxides, but resulted in non-stoichiometric materials with large amounts of the nitrate and carbonate radicals as impurities. The quantities of these impurities is sufficiently great in typical cases that we will refer to them as NiO* and CoO*, where the asterisk indicates that these are not pure stoichiometric materials. We will show that the main features of the original MO model are still indicated in that Schottky defects are the main cause of the observed differences between high and low temperature forms. The charge stabilization of the Fe^{3+} ion by electron trapping at negative ion vacancies originally proposed by MO is consistent with the present data, and we do not require an explanation

based on stoichiometric variations. We will show that porosity, neglected in the original model of MO, is necessary for a satisfactory description of the present data. Also, we will show that the observed increase in intensity of the Fe^{3+} resonance in CoO(I,II) or NiO(I,II) with temperature does not require a dispersal of oxygen vacancies as first suggested by MO[11].

Following up earlier work on CoO[6,11,14], we have applied simultaneous Mössbauer, x-ray, and chemical methods to NiO, and we have extended the earlier measurements on CoO. In particular we have performed gas adsorption measurements which were valuable in estimating porosity effects. We have also extended the measurements with applied magnetic fields and have studied superparamagnetism in these materials. We attempted to make direct measurements of particle size effects by preparing samples with the silica gel technique.

One of the most fruitful and interesting new techniques of investigating these oxides has involved the substitutional doping of cations of 1+ and 3+ valence, especially Li^{1+}, in the oxides. Significant changes in the ratio of the Fe^{3+} to Fe^{2+} resonance have been observed, as a result of doping, which are discussed from the semiconducting model of these materials. By comparing the Néel temperatures of doped and undoped samples, an estimate of the ratio of porosity to point defects in these oxides has been made. By comparing the Mössbauer characteristic temperatures of resonances in doped and undoped samples, confirmation of the structural differences of high and low temperature forms has been made. The doping experiments have also shed light on the unusual behavior of the Fe^{3+} resonance in mixed

forms CoO(I,II) and NiO(I,II). A practical application of Li^{1+} doping in CoO has been the preparation of a compact single-line source.

II. THEORY

A. Recoil-free Fraction

The probability that the nucleus will emit or absorb a gamma ray without a change in the phonon states of the crystal is known as the recoil-free fraction f. Using the quantum mechanical formalism of the interaction of radiation with matter, the quantity f can be shown[16] to be given by

$$f = \left| \langle n | \, e^{i\vec{\kappa}\cdot\vec{r}} \, | n \rangle \right|^2 ,$$

where $|n\rangle$ is an eigenstate of the lattice (which is unchanged in the emission process), $\vec{r}$ is the displacement vector of the nuclear motion, and $\vec{\kappa}$ is the momentum vector of the gamma ray divided by $\hbar$. If the interatomic forces of the solid are harmonic, the matrix element may be simplified to give

$$f = \exp(-\kappa^2 \langle u^2 \rangle) ,$$

where u is the displacement of the atom in the direction of emission of the gamma ray. The standard practice is to regard the crystal as a Debye solid with a characteristic Mössbauer temperature, θ_m , analogous to the Debye temperature, θ , determined from specific heat theory. The Debye model is strictly applicable only to monatomic lattices with a Debye phonon spectrum, but this method has proved to be useful in characterizing the recoil-free fraction f, even for

impurities in complex host lattices. It should be noted that θ_m and θ may have different values if the binding of the Mössbauer ion is quite different from the host ions. Using this Debye approximation the value of f becomes

$$f = \exp\left[\frac{-3R}{2k\theta_m}\left(1 + 4\,\frac{T^2}{\theta_m^2}\int_0^{\theta_m/T}\frac{x\,dx}{e^x-1}\right)\right] ,$$

where R is the recoil energy, k is the Boltzmann constant, and T is the absolute temperature. For values of T such that $T < \theta_m/2$, the integral may be approximated by its limiting value as $T \to 0$,

$$\int_0^{\infty}\frac{x\,dx}{e^x-1} = \frac{\pi^2}{6} ,$$

giving

$$f = \exp\left[\frac{-3R}{2k\theta_m}\left(1 + \frac{2\pi^2T^2}{3\theta_m^2}\right)\right] .$$

Since the area under the Mössbauer absorption spectrum is proportional[17] to f, it is common practice to plot ln A versus T^2 using the following relation

$$\ln A = C + BT^2 ,$$

where B and C are constants and B gives θ_m through the relation

$$B = \frac{-R\pi^2}{k\theta_m^3} .$$

Thus, the slope of the curve obtained will yield the value of θ_m . A more accurate method which is applicable for all values of T is to

calculate the integral

$$\int_0^{\theta_m/T} \frac{x\,dx}{e^x - 1}$$

numerically by computer. In the present work a computer program was used which found the best value of θ_m from the data points of area versus temperature, calculating the exact value of the integral when needed.

B. Magnetic Hyperfine Interaction

A magnetic field at the nucleus interacts with the magnetic dipole moment of both the ground and excited states, and the interaction is described by the following Hamiltonians:

$$\mathcal{H}_e = - g_1 \mu_N \vec{H} \cdot \vec{I} \quad , \quad \text{and} \quad \mathcal{H}_g = - g_0 \mu_N \vec{H} \cdot \vec{I} \quad ,$$

where g_0 and g_1 are the nuclear gyromagnetic ratios of the ground and excited states respectively, μ_N is the nuclear Bohr magneton, $\vec{I}$ is the nuclear spin, and $\vec{H}$ is the magnetic field at the nucleus. The eigenvalues of this type of Hamiltonian are:

$$E_m = - g \mu_N m H \quad ,$$

where m is the magnetic quantum number. In the case of Fe^{57} the excited state is split into four states, and the ground state is split into two states. Of the eight possible transitions between the excited and ground state levels two are forbidden by the selection rule for magnetic dipole transitions, ($\Delta m = \pm 1, 0$). Once the line positions

and therefore the relative energies of the six lines of a magnetic hyperfine spectrum have been measured, the value of H can readily be determined by a best fit of the data. The value of the gyromagnetic ratio of the ground state of Fe^{57} is known from nuclear magnetic resonance experiments.[18]

C. Superparamagnetism

If the average particle size of a powder sample becomes small enough (roughly of the order of 100 Å) the thermal energy of the particle can play a significant role in its magnetic behavior, because the spin orientation in a small particle can change due to thermal relaxation[19,20]. Néel derived the condition under which an assembly of such particles would come to thermal equilibrium in a given time, and the relaxation time for this process is:

$$\tau = \frac{1}{f_o} e^{KV/kT} \quad ,$$

where the frequency factor, f_o, is of the order of 10^9 sec^{-1}. K is the anisotrophy energy per unit volume depending upon such things as the external shape and imposed stresses of the particle, and it is assumed that each particle is a single domain with two anti-parallel easy directions. The source of the exponential arises from a simple statistical argument of the type used in reaction rate theory, where in the present case the energy barrier is KV . If the superparamagnetic relaxation time is long compared to the Larmor precession time, τ_L, of the first excited state of the Fe^{57}, a six-line magnetic hyperfine pattern will be observed below the Néel temperature. If τ and

τ_L are comparable a partial collapse of the magnetic hyperfine pattern will be observed, and as τ becomes less than τ_L the pattern will be converted to a broadened single line.

An applied external magnetic field will increase the superparamagnetic relaxation time. This is because fine particles, even though antiferromagnetic, have permanent magnetic moments, which are generally parallel to the alignment of the antiferromagnetic spin system and which result from an imperfect compensation of the magnetic sublattices. Such moments depend on the lack of structural perfection and on the surface form of the particle, and the moment will be larger as the particle size decreases. If the strengths of the six-line pattern and the unresolved broad single line are comparable, the application of an external magnetic field would be expected to convert some of the broad pattern into the resolved pattern for particles which are sufficiently small.

It has been estimated[14] that the energy of the magnetic moments of CoO or NiO microcrystals of order 50 Å, in an external field H_o of order 50 kG, is the same order of magnitude as the thermal energy kT at 100 - 300°K. This is the condition which must be satisfied if a large change in the relaxation time of microcrystals in an external field is to be seen.

D. Néel Temperature

Néel developed the theory of antiferromagnetism treating the case in which the exchange interaction is negative instead of positive.[21] Néel's theory, a generalization of the Weiss molecular field theory,

predicted a completely ordered spin arrangement at absolute zero, with two spontaneously magnetized equivalent sublattices. The directions of the ordered spins in the two sublattices are anti-parallel to each other. As the temperature is raised, the spontaneous magnetization decreases and goes to zero at a transition temperature usually called the Néel temperature, T_N. A simple two-sublattice model predicts that $\theta_p/T_N = -1$, where θ_p is the paramagnetic Néel temperature used in the Curie-Weiss law; but this two-sublattice model fails for compounds such as NiO or CoO, which have face-centered cubic lattice arrangements. For the fcc arrangement two nearest neighbors of a given atom can themselves be nearest neighbors. The simple two-sublattice model also fails for CoO and NiO, because it does not consider second and more distant neighbor exchange interactions. The difference between the paramagnetic Néel temperature, θ_p, and the Néel temperature, T_N, can be quite large.

There has been some controversy over the actual arrangement of spins in antiferromagnetic CoO, as has been recently discussed by Khan and Erickson.[22] In what follows, the assumption of a single spin axis, as opposed to multispin axes, will be made. We will assume the simpler model for purposes of investigating the possible effect of impurities and cation vacancies on the Néel temperature. The basic conclusion should not be changed by the complication of a possible multispin structure.

Following an analysis by Smart,[21] using the generalized molecular field theory approach, the Néel temperature can be written as

$$T_{N_s} = \frac{C}{n} \sum_{j=1}^{n} n_{ij} \gamma_{ij} \quad ,$$

where i and j refer to spin sublattices, and where $n_{ij} = 0$ or ± 1 reflects the relative spin arrangements between the i and j sublattices. The value of γ_{ij} is

$$\gamma_{ij} = C' z_{ij} J_{ij} ,$$

and C and C' are constants. The value of γ_{ij}, the molecular field coefficient for the field exerted on an atom of the i sublattice by its neighbors in the j sublattice, is thus proportional to z_{ij}, the number of j neighbors of an i atom, and the exchange interaction between and i atom and one of its j neighbors, J_{ij} . The number of sublattices is n, and the subscript s in the term T_{N_s} is an index which labels which of the transition temperatures, corresponding to the different types of possible antiferromagnetic ordering, is being discussed. Some of the types are usually translationally degenerate. The solutions of T_{N_s} for the face-centered cubic lattice correspond to three values of the Néel temperature, because there are three possible types of antiferromagnetic ordering for this lattice arrangement. The three solutions may be written as follows:

$$T_{N_1} = C''(-\tfrac{1}{3}\gamma_1 + \gamma_2)$$

$$T_{N_2} = -C''\gamma_2$$

$$T_{N_3} = \tfrac{1}{3}C''(-\gamma_1 + \gamma_2) ,$$

where γ_1 denotes the molecular field coefficient for the 12 nearest neighbors, γ_2 denotes the molecular field coefficient for the 6 second

nearest neighbors, and C'' is a constant. The type of ordering predicted from theory and also experimentally observed for NiO and CoO is of the second type. This second type corresponds to a magnetic structure in which there are four independent antiferromagnetic simple cubic lattices, where each cation has six anti-parallel second nearest neighbors and is completely uncorrelated with its nearest neighbors. For the uniaxial model assumed, a set of planes perpendicular to a cube diagonal are ferromagnetically ordered, with the spin direction of adjacent planes being anti-parallel.

Therefore, the value of T_N for NiO and CoO is

$$T_N = C_1 z_2 J_2$$

where z_2 is the number of second nearest neighbors, J_2 is the exchange interaction between second nearest neighbors, and C_1 is a constant. It is reasonable to expect, therefore, that if 1% of the nickel or cobalt atoms in an oxide sample are randomly replaced by a substitutional dopant such as lithium, the value of T_N will be lowered by approximately 1%. An average performed over z_2, the number of second nearest neighbors, will be less than the normal value by 1%. This has been experimentally observed for 1% dopings of Li in both CoO and NiO, as will be discussed in Section V-E. Therefore, this derivation based on a single spin axis model confirms the plausibility of the experimental results for lithium doped samples. Nickel or cobalt vacancies would also be expected to lower the Néel temperature in a similar manner, as long as the number of these point defects is small compared

to the number of cobalt or nickel ions. This latter condition is only roughly satisfied in CoO(II) and NiO(II), as will be shown later.

III. EXPERIMENTAL TECHNIQUES

A. Mössbauer Spectrometry

The majority of the data were taken with a mechanical velocity spectrometer which produced a crank motion at the absorber.[23] A schematic drawing of the mechanical system and the accompanying electronics is shown in Fig. 2. This type of spectrometer is a rapid scan device in that it repetitively scans through the entire range of velocities in a time interval (~ 1 sec) short compared to typical electronic drifts. A synchronous motor and a 100:1 gear reducer, mounted on a separate table to avoid vibration, provided power for the crank assembly through a Tilton elastic belt. Various pulleys, which were concentric to 0.0002 inch, were attached to the motor system output and to the crank assembly to give various velocity limits. Large flywheels were connected to the motor output and crank assembly to insure a uniform rate of rotation, which was experimentally verified to within ± 0.5%, as measured with a photodiode gating circuit. The absorber was attached to the reciprocating shaft driven by the crank arm connected to the flywheel. The flywheel turned with a constant angular speed ω, and the velocity of the absorber as a function of θ could be calculated from the geometrical constants of the crank assembly, a and b. While the absorber moved back and forth through a range of velocities, the 14.4 keV gamma rays transmitted through the absorber were analyzed by a gas-filled proportional tube,

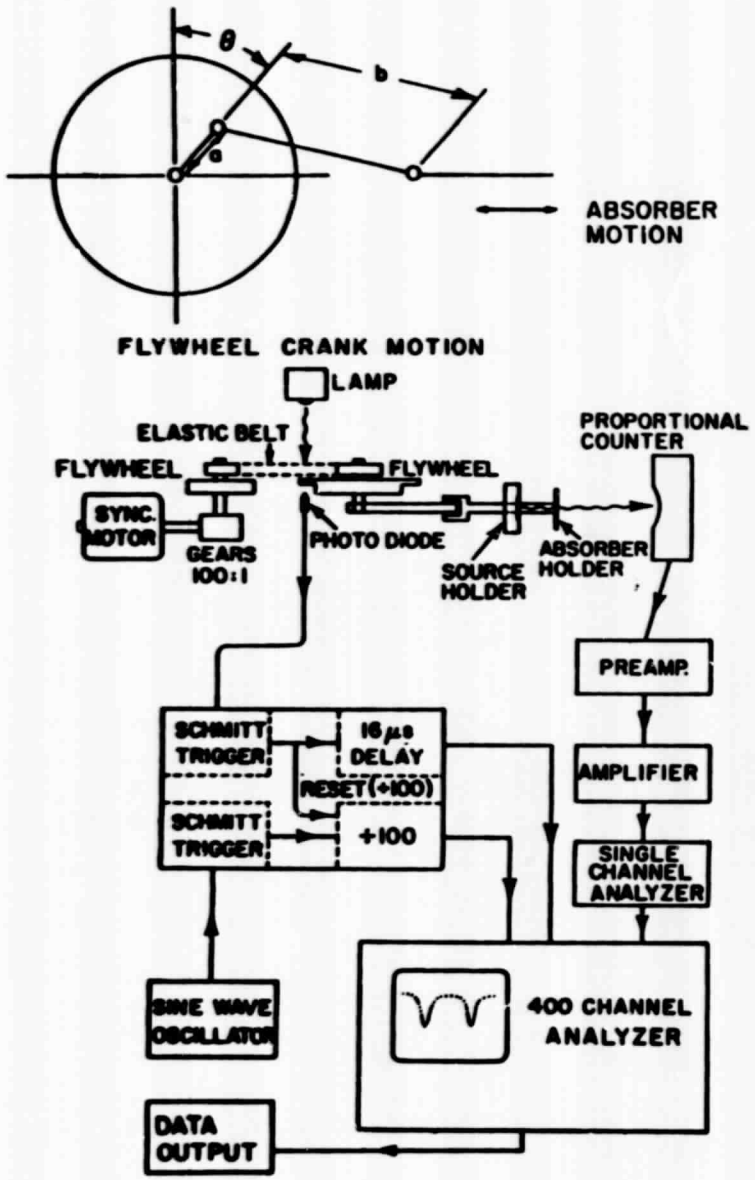

Figure 2. Schematic diagram of Mössbauer spectrometer.

preamplifier, amplifier, and a single channel analyzer. The gamma rays were counted and stored in a 400 channel RIDL multichannel analyzer operated in the multichannel scaler mode. The sine wave output of an independent oscillator was converted by a Schmitt trigger and two decade scalers into approximately 200 evenly spaced pulses per crank revolution which advanced the channel address. Each channel of the analyzer therefore represented the count rate at a certain velocity of the absorber. The multichannel analyzer was reset synchronously with the reciprocating motion by a pulse from a photodiode, and synchronism in the reset was kept to within 0.01 channel by operating the sine wave oscillator at 100 times the channel - stepping frequency. A small phase angle parameter was determined which gave the best overlap of the mirror image spectra stored in the analyzer. The frequency of crank rotation and of the channel stepping oscillator were measured by counting the pulses in a timer-scaler unit. The output of the analyzer could be converted, therefore, into a record of gamma ray transmission through the absorber as a function of absorber velocity. A very small amount of data was taken with an automated constant velocity spectrometer.[24] This spectrometer had a unique feature which allowed a selection of velocities with a programmed paper tape. This type of spectrometer has the advantage that a spectrum can be taken with fewer points and in the region of interest only.

The temperature of the source could be varied with a dewar-heater arrangement. For low temperatures the source was attached to a copper block on the bottom of the dewar filled with a coolant. An insert in the copper block, for a Watlow heater rod, made it possible to warm

the block relative to the coolant temperature. By using the Watlow heater without a coolant, temperatures above room temperature could be maintained. A temperature controller, manufactured by the Barber-Colman Company, was used for controlling temperature within ± 1°C. Temperature measurement was made with calibrated thermocouples.

For experiments involving sources, narrow unsplit sodium ferrocyanide absorbers ($Na_4Fe(CN)_6 \cdot 10\ H_2O$) of various effective thicknesses were used (0.1, 0.25, 0.75, and 1.0 mg/cm^2 Fe^{57} concentration), purchased from New England Nuclear Corporation. The standard absorbers were kept at room temperature while the temperature of the source was varied. For experiments involving the preparation of a Fe^{57} doped NiO or CoO absorber, standard unsplit sources with a Pd or Cu host matrix were used.

B. Sample Preparation

Cobaltous oxide and nickelous oxide are frequently prepared by heating the various salts of cobalt and nickel, such as the carbonate or nitrate, to temperatures above 250°C in various atmospheres. They can also be prepared by heating the metal in an oxidizing atmosphere such as oxygen or carbon dioxide[25,26]. In general, the properties of the oxide formed appear to be influenced more by the annealing temperature and atmosphere than the choice of starting materials. MO prepared CoO(II) by decomposing $CoCO_3$ in vacuum at 300°C or by reducing a higher oxide, formed from a nitrate, in hydrogen at even lower temperatures. CoO(I) was prepared by oxidizing Co metal in a carbon dioxide atmosphere at 1000°C in a sealed quartz tube, and CoO(I, II)

was prepared by heating cobalt metal or cobaltous nitrate in air at 1000°C. The high temperature samples were quenched in an inert atmosphere from 1000°C to 0°C to 77°K. The samples of cobaltous oxide needed in this investigation were prepared using the methods of MO.

We attempted to prepare NiO(II) by heating nickelous nitrate in various atmospheres at temperatures from 250°C to 400°C. Some experiments were carried out on samples prepared around 300°C in vacuum, and more extensive experiments were carried out on samples prepared at 400°C in argon. The starting material of 99.999% pure nickel metal was dissolved in nitric acid, and carrier free, radioactive Co^{57} was added to the solution in the form of $CoCl_2$. The solution was dried on a hotplate and then annealed in a horizontal glass tube in the desired atmosphere. After losing the water of hydration, the nitrate decomposes as follows:

$$2\ Ni(NO_3)_2 \longrightarrow 2\ NiO + 4\ NO_2 + O_2 \ .$$

The horizontal glass tube was placed inside a cylindrical piece of inconel in the furnace in order to reduce thermal gradients, as shown in Fig. 3. A vacuum pump, a mercury manometer, and gas tanks were used as necessary to maintain the atmosphere used in the sample preparation. The samples were kept in an inert atmosphere, such as argon, using a glove box and sealed sample holders until it was determined that the low temperature preparations of nickelous oxide did not pick-up oxygen as did the low temperature cobaltous oxide samples. Only those samples annealed at 400°C for several hours (5 to 10) yielded the pure stoichiometric NiO(II). Those annealed at 300°C generally

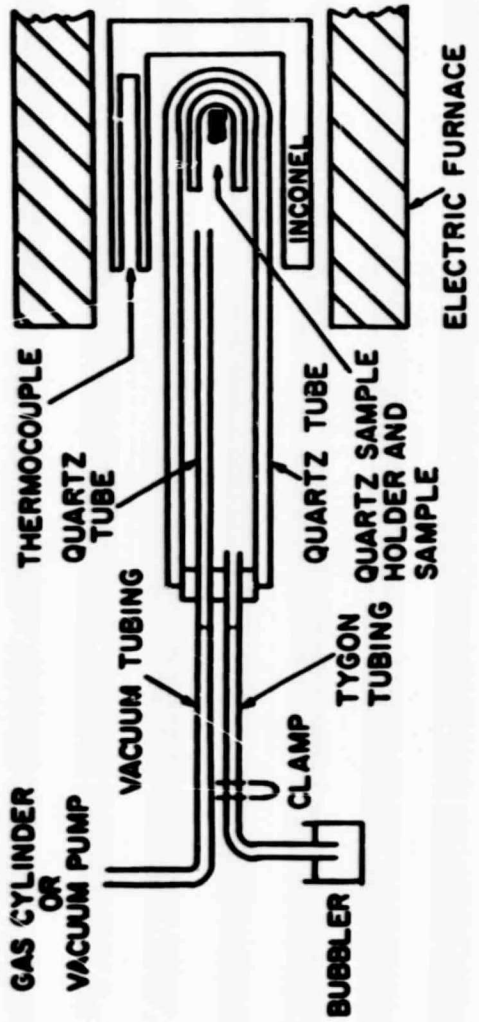

Figure 3. Schematic diagram of sample preparation.

gave considerable deviation from stoichiometry and were found to contain appreciable nitrate impurity. These latter impure specimens are referred to as NiO* and are discussed in greater detail in Section IV.

For samples containing dopants of other cations, the dopant was added in the form of its nitrate to the initial solution of nickelous or cobaltous nitrate. This insured that the dopant was initially dispersed before the annealing process. To avoid the added complications found for low temperature preparations, all of the doped samples were prepared at elevated temperatures similar to form I preparations. The small amounts of dopants added necessitated careful weighing on a Mettler semimicro balance, and often a larger amount of the nitrate of the dopant was diluted with water and an appropriate aliquot taken. Otherwise the doped samples were prepared in an identical manner to the undoped form I samples. Mössbauer spectra of the doped samples indicated that the dopants dispersed into the CoO and NiO lattices, and other investigators[27-29] have indicated that the dopants occupy substitutional sites randomly dispersed within the host lattice without affecting the crystal structure. X-ray diffraction patterns of doped and undoped samples were the same within experimental errors.

C. X-ray Technique

The x-ray diffraction patterns of various samples were made on a powder diffractometer made by the North American Philips Company. Either Mo Kα radiation (Kα_1 = 0.70926 Å and Kα_2 = 0.71354 Å) or Cu Kα radiation (Kα_1 = 1.54050 and Kα_2 = 1.54434 Å) was used to yield the Bragg peaks. The Mo tube was used with a zirconium filter which

absorbed about 96% of the Kβ line[30], and the Cu tube was used with a nickel filter to absorb about 98% of the Kβ line. The operating voltage and current of the Mo tube were set at 40 kV and 15 mA, and the Cu tube was run at 35 kV and 15 mA. The NiO samples could be examined with either tube, but the CoO samples could not be measured with the copper tube because the Cu Kα radiation will excite the fluorescence lines of the K series of cobalt.[31] A Geiger counter and chart drive were used to record the Bragg peaks and the diffractometer had provisions for using various scanning speeds and beam slits. The electronics of the Geiger tube circuit allowed a selection of time averaging to smooth out the counting current. Plexiglass specimen holders constrained the sample to a disk of diameter 10 mm and a thickness of 1 mm, which was greater than the minimum thickness required for maximum diffracted intensity.[30]

D. Gas Pickup and Surface Area Measurements

The holder used in the gas pickup and surface area measurements is shown in Fig. 4. The volume of the container was approximately 25 cm^3, and the weight of the entire holder was approximately 40 g. The holder weight was kept down by using aluminum in the bottom so that with 10 g of the sample the total weight was small enough to be measured on the Mettler semimicro balance. The holder could be sealed by placing a wire clip on the tygon tubing at the top of the holder, and a piece of rubber maintained the seal between the top and bottom. Since the container could be evacuated or filled with a gas through the tygon tubing on the top without transfer to a glove box, the process

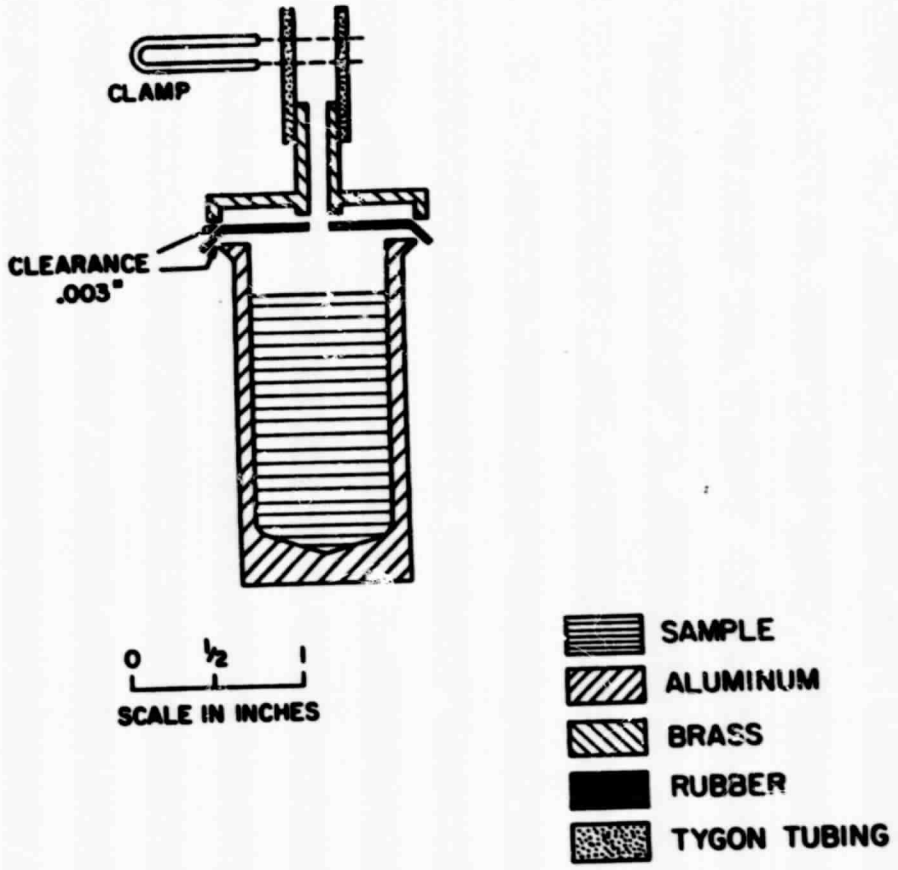

Figure 4. Holder for gas pickup and surface area measurements.

of weighing the sample in various atmospheres could be performed within a few minutes. It was experimentally verified that the vacuum seal of the holder was adequate by observing the weight of the evacuated holder over a period of ten minutes. During the processes of filling and transfer to the balance, the holder was handled with plastic gloves to give the accuracy needed in weighing.

E. Particle Size and Superparamagnetism Studies

In a few experiments an external magnetic field H_o was applied to a source. This external magnetic field was produced by a superconducting magnet designed by the Eastern Scientific Company with a dewar made by Janis Company. The direction of the field was along a horizontal axis, and the absorber was moved along this same axis. The superconducting magnet was capable of fields up to about 55 kG, and it had been calibrated with a rotating coil gaussmeter. The dewar, whose hold time was 6-8 hours, had provisions for mounting the source on the helium jacket, the nitrogen jacket, or on the outside at room temperature. In order to restrict the particle size of one sample used in the magnetic studies, the preparation was carried out in silica gel which had been supplied by the W. R. Grace Company. The particular grade used, No. 59, had an average pore diameter of 140 Å and was 99.5% SiO_2 with a small amount of impurities, mainly Al_2O_3. The silica gel was heated initially to remove water vapor and then allowed to pickup by capillary action the solution of nickelous nitrate into its pores. The resultant heating of the sample at 600°C produced NiO with an upper bound on the average particle size of 140 Å.

IV. X-RAY AND CHEMICAL MEASUREMENTS

A. Stoichiometry

The stoichiometries of the cobaltous and nickelous oxide samples were determined by a direct gravimetric measurement. Samples were weighed, reduced to metallic form by heating in hydrogen at 500°C, and then weighed again. MD showed that CoO(I), CoO(II), and CoO(I,II) were all nominally stoichiometric, and the results of measurements on the nickelous oxide system are shown in Table 1. The two low temperature preparations for NiO listed were checked independently for undecomposed nitrate, which was being sought as a possible contaminant from the starting material of nickel nitrate. A typical sample of the first preparation listed (prepared at 300°C) having an indicated stoichiometry of $NiO_{1.4}$ was analyzed for nitrate in a microanalysis laboratory in the chemistry department of Purdue University. The result of this analysis indicated that about half of the indicated excess stoichiometry was due to undecomposed nitrate, and therefore the stoichiometry of the sample would be $NiO_{1.22 \pm .05}$ if the nitrate were accounted for. A typical sample of the second preparation listed (prepared at 400°C) was sent to the Schwarzkopf Microanalytical Laboratory in Woodside, New York, which was equipped to test for smaller quantities of nitrate. The result of their analysis on a sample of $NiO_{1.02 \pm .02}$ indicated that the percent of nitrogen by weight was zero or less than 0.008%.

Table 1

Stoichiometry of nickelous oxide. Gravimetric determinations of x, written as NiO_x.

NiO* a)	NiO(II) b)	NiO(I) and NiO(I,II)
1.39 ± .02	1.01 ± .02	.99 ± .01
1.22 ± .02	1.03 ± .02	.99 ± .01
1.09 ± .02	1.02 ± .02	1.00 ± .01
1.16 ± .02	1.01 ± .02	

a) These samples were prepared at 250-350°C in vacuum. Microanalysis indicated that about half of the indicated excess stoichiometry was due to undecomposed nitrate from the starting material of nickelous nitrate, as discussed in the text.

b) These samples were prepared at 400°C in argon. Microanalysis indicated that these samples were essentially free of undecomposed nitrate.

The results of the microanalysis therefore indicate that the first preparation listed has some undecomposed nitrate still in it, but that the second preparation listed is essentially free of undecomposed nitrate. The analyses for nitrate were carried out using the standard Dumas method[32] for determining nitrogen content. The sample was mixed with powdered cupric oxide and ignited in a stream of CO_2 gas in a combustion tube, and any nitrogen was converted primarily to the elemental state with a small amount of oxides of nitrogen. The nitrogen oxides were reduced to elemental nitrogen by passing the gases over a bed of hot copper. The products of the ignition were then swept into a gas buret filled with highly concentrated KOH which completely absorbed CO_2, H_2O, and other products of combustion. N_2 remained undissolved in the KOH solution and its volume was directly measured.

B. Density

One of the interesting and pertinent differences between the low and high temperature preparations of these oxides is the density, as measured by the standard volume-gravimetric technique. MO showed that CoO(I) had a density of 6.4 ± .1 g/cm^3 as predicted from its known NaCl structure and its lattice parameter of 4.25 Å[33]. They found that CoO(II) had an average density of only 4.8 ± .5 g/cm^3. These density measurements were made on large samples (of order 3g). Our results have demonstrated that their basic method can be reliably used on smaller samples (of order 300 mg) to substantiate that the Mössbauer samples of CoO(II) have the same average density as the larger samples. We have also found that NiO samples can exhibit an analogous lowering of

density as shown in Table 2. The average density of NiO* samples prepared at 250-350°C was found to be 5.1 ± .2 g/cm^3, and the average density of NiO(II) samples prepared at 400°C was found to be 6.0 ± .2 g/cm^3. The density of NiO(II) samples therefore is about 12% below the value of 6.8 g/cm^3 based on a perfect NaCl structure of NiO(I) and a lattice constant of 4.19 Å[34,35].

The density measurement technique was the standard volume-gravimetric approach using carbon tetrachloride as a non-reactive liquid in which the sample was immersed in a volumetric flask. The necessary weighings were made on a Mettler semimicro balance, and the CCl_4 used in the measurements was high purity Mallinkrodt spectrophotometric grade of density 1.584 ± .001 g/cm^3, which was checked against the same volume of triply distilled water. The density of standard materials such as NaCl and Ni in amounts as small as 0.06 ml, corresponding to about 300 mg of NiO(II) or CoO(II), were measured to within about 4% of the expected values, and for larger samples of order 2 g or more the accuracy was within 2%. The accuracy in density measurement achieved with the samples of order 300 mg required careful handling of the volumetric flask with plastic gloves during the weighing process, and a syringe was used to add the CCl_4 to the flask. The exact volume of the volumetric flask was measured before the sample was added, and the samples immersed in the CCl_4 were evacuated with a fore pump in an attempt to eliminate gas bubbles.

It is natural to ask whether a density measurement made with a liquid such as carbon tetrachloride on CoO(II) or NiO(II) samples reflects a density lowering due only to point vacancies and whether it

Table 2

Densities of CoO and NiO. Density measurements in g/cm^3.

Sample Size	CoO(II)	NiO* a)	NiO(II) b)
~ 300 mg	4.7 ± .2	4.7 ± .2	6.0 ± .2
	5.0 ± .2	5.3 ± .2	
		5.0 ± .2	
~ 2 g		5.4 ± .1	5.9 ± .1
			6.1 ± .1

a) These samples were prepared at 250-350°C in vacuum.

b) These samples were prepared at 400°C in argon.

would also reflect porosity or holes resulting from a microcrystal structure. Schroeer and Triftshauser suggested that the carbon tetrachloride could not get into small pores in the samples because of surface tension. When these density measurements were correlated with subsequent Mössbauer and gas adsorption measurements, it became apparent that the density lowering was a result of both point defects and porosity. An estimate of the fractional partitioning between point or Schottky defects and porosity was obtained from Mössbauer data and will be discussed in Section VI.

C. X-ray Patterns

The x-ray diffraction technique is a useful tool for determining the composition of a sample, for estimating particle size, and for observing changes in the lattice constant of materials.[30,31,36] MO found that the x-ray diffraction patterns of CoO(I) and CoO(II) had essentially identical line positions and relative intensities. The diffraction peaks for CoO(II) were broader, however, and this broadening gave an estimate of a domain size in CoO(II) of order 50 Å. The absence of extra lines in the x-ray diffraction pattern of CoO(II) indicated that there was no long range ordering of vacancies. This was plausible because of the many different possible arrangements of vacancies. Similar results have been found for samples of NiO as shown in Fig. 5. X-ray diffraction patterns are shown for samples of NiO* and NiO(II) prepared at 300°C and 400°C, and for NiO(I) prepared at 1000°C. CoO(I) and NiO(I) are isomorphous , having the NaCl structure with the following coordinates:

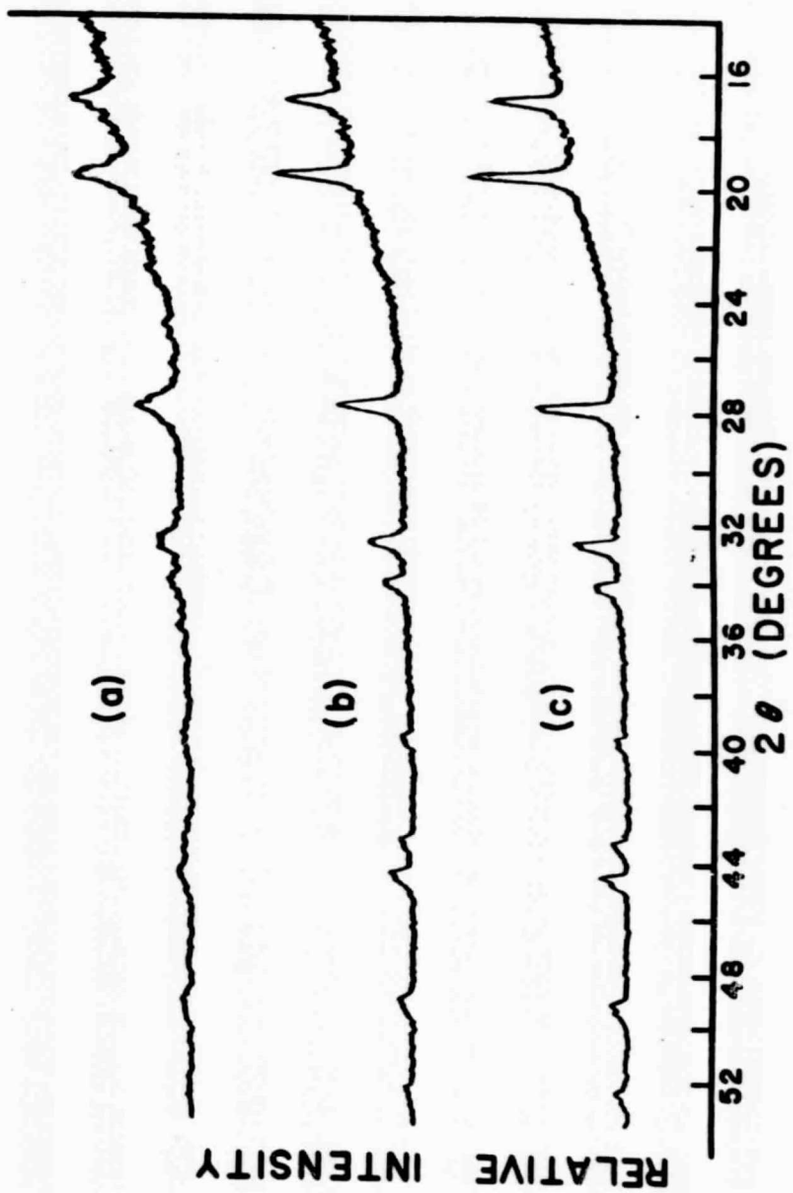

Figure 5. X-ray diffraction patterns for (a) NiO* prepared at 300°C, (b) NiO(II) prepared at 400°C, (c) NiO(I) prepared at 1000°C, using Mo Kα radiation.

Co or Ni (000), $(0\frac{1}{2}\frac{1}{2})$, $(\frac{1}{2}0\frac{1}{2})$, $(\frac{1}{2}\frac{1}{2}0)$

O $(\frac{1}{2}00)$, $(0\frac{1}{2}0)$, $(00\frac{1}{2})$, $(\frac{1}{2}\frac{1}{2}\frac{1}{2})$.

Using the spacings of the crystal planes,[37] d, the x-ray peak positions were calculated using Bragg's Law with Mo Kα radiation, and the results are given in Table 3. Within experimental errors the experimental peak positions were the same as the calculated ones. The broadening of the NiO* and NiO(II) diffraction patterns, as compared with the pattern for the high temperature sample, was used to obtain an estimate of particle size. The mean dimension D_c of a crystallite composing a powder is related to the pure x-ray diffraction broadening β (in radians) as follows:[30]

$$D_c = \frac{C\lambda}{\beta\cos\theta} .$$

where D_c represents the average length over which x-rays are scattered coherently, C is a constant approximately equal to unity for different crystallite shapes, and θ is the diffraction angle. β is the pure breadth of a powder reflection free of all broadening due to the experimental method, and it is related to the experimentally observed breadth B in the following way:

$$B^2 = \beta^2 + b^2$$

The width of the particular line being considered in a high temperature form, b, serves as a standard since it is assumed to represent the broadening due to experimental geometry and electronics, without any

Table 3

Bragg peak positions for NiO using Mo Kα radiation.

HKL	d(Å)	2θ
111	2.410	16.93
200	2.088	19.56
220	1.476	27.82
311	1.259	32.73
222	1.206	34.20
400	1.044	39.70
331	.958	43.44
420	.934	44.66
422	.853	49.12
511	.804	52.30

particle size effects. The results of this analysis applied to the three patterns shown in Fig. 5 indicated that the particle size was of the order of 100 Å for the first sample, NiO* (prepared at 300°C), and of the order of 200 Å for the second sample, NiO(II) (prepared at 400°C). It should be stated that this x-ray particle size method has some limitations in absolute accuracy because of variations in crystallite shapes, geometry, and electronics used. It is very good, however, for comparing the relative particle size of a series of samples.

In order to learn more about the mechanism of oxygen pickup in CoO(II), x-ray diffraction measurements were correlated with the amount of oxygen picked up. Fig. 6 shows the x-ray powder pattern for CoO(II)· nO as a function of n. It should be noted that the oxygen pressure had to be increased slowly in order to avoid a strong exothermic reaction that would convert the CoO to Co_3O_4 . In the early stages of oxygen pickup the x-ray pattern is practically unchanged within experimental errors, although in the latter stages ($n \geq .3$) the relative intensities change, the positions of the lines shift slightly, and the lines begin to broaden. The point at which the x-ray pattern begins to change significantly corresponds to a rather sharp knee in the curve representing the time dependence of the oxygen pickup. The sharp knee in the n(t) curve with the accompanying x-ray pattern changes seems to indicate that the oxygen pickup is a two stage process. The results are suggestive of an initial surface pickup or oxidation followed by a slower diffusion of the oxygen into point oxygen vacancies in the sample. The density of Schottky defects, however,

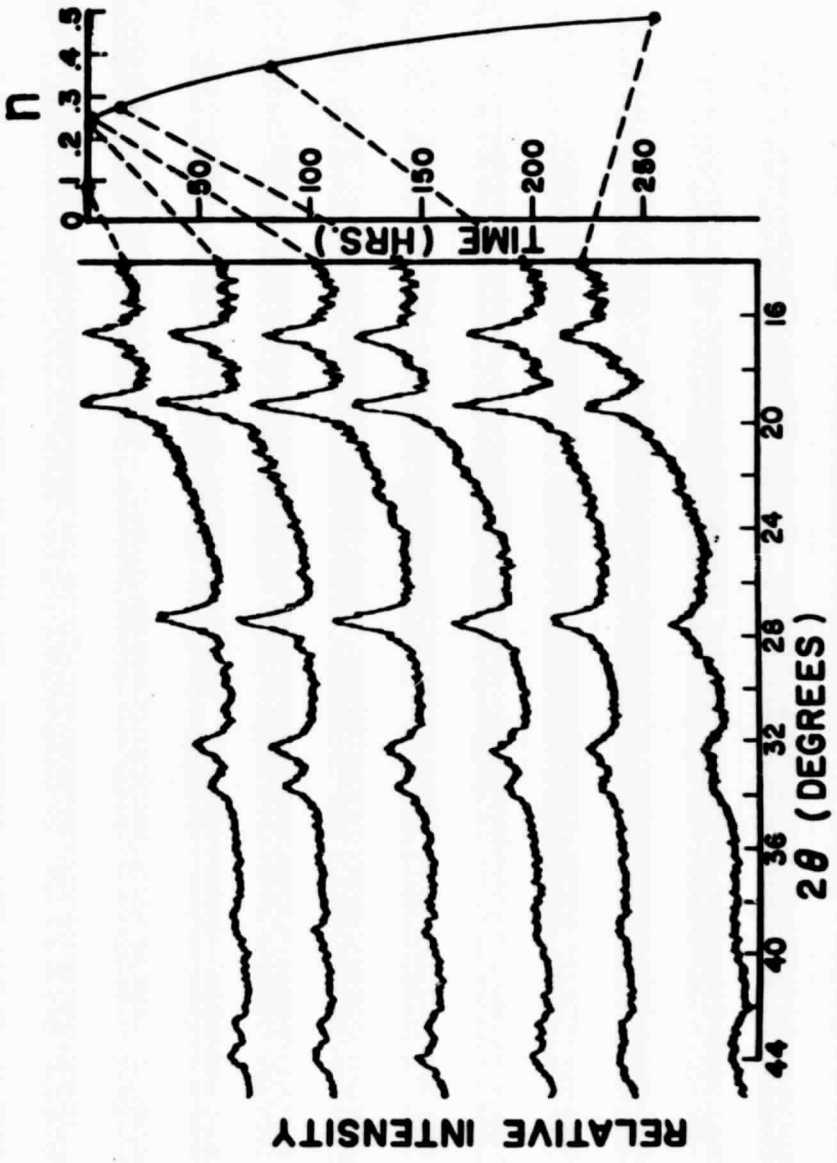

Figure 6. X-ray diffraction patterns for CoO(II)·nO as a function of n.

which is shown in Section VI to be of order 6% of the lattice sites, does not appear to be great enough to account for the large O_2 pickup after the knee of the n(t) curve is reached. Thus, even this rather involved picture is unable to explain the large remnant CoO(II) Mössbauer pattern[11,14] after the O_2 content has increased by 50 to 60%. Also, it is not clear why the changes in the Mössbauer pattern upon oxidation of CoO(II) do not appear to reflect a two stage process, although this might be accountable on the basis of a resolution problem in the first stage of O_2 pickup. Whatever the detailed mechanism of oxygen pickup, the results appear to require a large surface area, which is consistent with a spongelike structure and an appreciable amount of Schottky defects. Further investigation will be required before the detailed mechanisms of oxygen pickup are fully understood.

D. Gas Pickup and Surface Area Measurement Results

The purpose of making measurements on samples in the holder described in Section III-D was to look for effects indicating a large surface area for CoO(II) or NiO(II) and to study the oxygen pickup of CoO(II) more carefully.

In order to study the pickup of oxygen by CoO(II) more carefully, a sample of approximately 10g was placed in the holder. The holder was then evacuated with a diffusion pump and weighed carefully on the semimicro balance. A very small partial pressure of oxygen was then admitted to the holder for a period of a few minutes, and upon evacuating the holder plus sample and weighing, it was found that the sample had picked up weight. This is in contrast to the pickup of

argon and neon, which will be discussed later in this section, in which the gas picked up could be reversibly removed by placing the sample under diffusion pump vacuum. This measurement shows that the oxygen pickup of CoO(II) in the early stages cannot be a physical adsorption, but must either be a chemical adsorption or process in which the oxygen diffuses into the lattice.

In contrast to the pickup of oxygen observed in CoO(II), measurements with Ar and Ne on CoO(II) and NiO(II) have demonstrated the well-known physical adsorption of gases, and these were used to estimate the surface area of the CoO(II) and NiO(II) samples. The holder and the weighing technique used in these measurements were checked by measuring the density of standards of large particle size such as Co and NaCl with gases. Since the densities of gases are lower by at least a factor of 1000 than liquids such as CCl_4, the measuring technique must be very precise. It is easy in theory to find a method for measuring the density of a sample with gases. We let W_1 denote the weight of the holder when filled with gas 1 (with density D_1) and W_2 denote the weight of the holder when filled with gas 2 (with density D_2). The volume of the holder is then

$$V_c = \frac{W_2 - W_1}{D_2 - D_1} \quad .$$

The measurement is repeated with a sample in the container. If W_3 is the weight of the holder plus sample in gas 2 and W_4 the weight of the holder plus sample in gas 1, then the volume of the holder minus that of the sample is

$$V_c - V_s = \frac{W_3 - W_4}{D_2 - D_1} \quad .$$

The volume of the sample is, therefore,

$$V_s = \frac{W_2 - W_1 - W_3 + W_4}{D_2 - D_1} \quad .$$

The weight of the sample can be shown to be

$$W_s = W_3 - W_2 + V_s D_2 \quad .$$

The density of the sample can therefore be found after algebraic manipulation to be

$$D = \frac{(W_2 - W_3)D_1 + (W_4 - W_1)D_2}{W_2 + W_4 - W_1 - W_3} \quad .$$

It should be noted that this formula is valid if either D_1 or D_2 is zero, which would correspond to the case in which one set of weighings is made in vacuum. The densities of the gases must be corrected to the temperature and pressure of the experimental environment. The densities of Co and NaCl of large particle size were measured by this technique and found to be reproducibly within about 5% of the theoretical values. This confirmed that the holder and weighing technique were accurate enough and reproducible.

When we applied this technique to study NiO(II) and CoO(II) we found that our measurements of the density of these materials, with

99.998% pure Ar and 99.995% pure Ne, gave results far outside the expected range.[38] The results were off in such a direction as to indicate that the samples had a large surface area, and therefore a large surface adsorption. This result was consistent with the x-ray patterns of CoO(II) and NiO(II) samples, indicating an x-ray particle size of the order of 100 Å in contrast to the standards Co and NaCl, which had very sharp x-ray diffraction peaks. By working back it was found that the density values would be in the correct range if the samples of NiO(II) and CoO(II), which were of order 10g, were physically adsorbing of the order of 4 mg of argon and .1 mg of neon, and it was experimentally verified that the argon and neon could be removed by pumping with a diffusion pump.

Surface adsorption can be of two types,[39] usually referred to as physical and chemical adsorption. In chemical adsorption a reaction takes place at the surface, and the gas generally cannot be pumped off by a diffusion pump vacuum. In physical adsorption a weak van der Waals force holds the gas atoms or molecules on the surface, and the gas can be pumped off with a diffusion pump vacuum. The amount of physical adsorption is related to the surface area of the sample and the critical temperature of the gas. Physical adsorption is nonspecific in that many gases may be physically adsorbed on a surface, but chemical adsorption is obviously more specific, which is demonstrated by the difference between the pickup of Ar and O_2 by CoO(II). The rate of adsorption is very rapid, because the gas atoms or molecules are adsorbed as soon as they reach the surface.

From the amount of gas adsorbed on the surface of a sample an estimate can be made of the surface area or average particle size. Above the critical temperature of the gas being adsorbed the molecules or atoms go onto the surface in a monolayer at most, but as the temperature approaches the critical temperature the fraction of the surface covered approaches 1. Since our observations of the adsorption of Ne and Ar were carried out at room temperature, which is well above the critical temperature of either gas, the fraction of the surface covered will be much less than 1. The area of a molecule or atom on the surface is usually approximated by assuming that the adsorbed molecules have the same packing on the surface as the molecules or atoms of the solidified gas in their plane of closest packing. Carrying out such a calculation for a 4 mg adsorption of argon on CoO(II) or NiO(II) led to an estimate of the particle diameter D_p of order of

$$D_p = \alpha(10{,}000\ \mathring{A}) \quad ,$$

where α is the fraction of a monolayer of gas adsorbed. An assumption of 1% of the surface being covered by Ar leads to an estimate of the particle size of the same order of magnitude as required to explain the x-ray peak broadening for these samples, discussed in Section IV-C .

V. MÖSSBAUER MEASUREMENTS

A. Reduction of Data and Error Analysis

The data output of the spectrometer was initially analyzed in a computer program, which computed the velocity in mm/sec and the percent absorption for each datum point. The baseline was estimated by an average of the points in the outer velocity limits, and a rough plot of the data was generated in the computer output. The program also calculated the area under the curve numerically using a trapezoidal area rule and determined the isomer shift. This initial data analysis gave estimates of the Mössbauer parameters such as peak positions, linewidths, and areas which were then refined in a curve fitting computer program.

The Breit-Wigner theory of radiation[40] predicts that ideally the curve representing nuclear resonant absorption will have a Lorentzian line shape, which is described by the following expression:

$$A(v) = \frac{S\Gamma/2\pi}{(v-v_o)^2 + \Gamma^2/4} = \frac{I(\infty) - I(v)}{I(\infty)} \quad .$$

The term A(v) represents the fractional effect or absorption as a function of absorber velocity, the term Γ is the full width at half maximum for the Lorentzian curve, and v_o is the velocity of the center of the peak. The area under the curve is S, which may be verified by

integrating A(v) over all velocities. I(∞) and I(v) are, respectively, the transmitted gamma ray intensity at velocity far removed from the center of the peak and the transmitted gamma ray intensity as a function of velocity. If the Mössbauer pattern consists of more than one line, for example a six-line magnetic hyperfine spectrum, the absorption curve can be expressed as a superposition or sum of the six individual Lorentzian curves.

The curve fitting of the Mössbauer data to a function as described above was done with a non-linear regression, least-squares computer program, which was capable of fitting experimental data to an arbitrary function of one or two independent variables and a large number of parameters. In actual practice, the experimental spectra were usually fitted with less than twenty parameters. The theory of a curve fitting program of this type is sophisticated, but in essence its function is to generate a curve which best fits the data as determined by a minimum of the sum of the squares of the residuals, deviations of the fitted and experimental points.

There was some error in determining the velocity and gamma ray intensity of each datum point. The error in the velocity using the crank spectrometer was a function of the uniformity of rotation of the flywheel, the accuracy to which the instrument was machined, and the measurement of the geometric crank parameters. The maximum error in the velocities is estimated to be 0.5% and should be less on the average. The emission and absorption of the gamma rays is described by Poisson statistics. There are various ways of expressing the error associated with Poisson statistics, but they all are related to the

value of $\sqrt{N}$ where N is the total number of gamma rays counted. The standard deviation of the counts at a particular velocity is $\sqrt{N}$, and the fractional standard error is $1/\sqrt{N}$. In most of the experimental data the value of N was greater than 10^5 for a fractional standard error of 3/1000. Since the Mössbauer absorption lines were typically 10%, the signal to noise ratio was typically 30 to 1. In order to maximize count rate, the single channel analyzer was set wider than the half maximum of the 14.4 keV peak. The gas filled proportional tube was run at the lowest voltage necessary to adequately resolve the 14.4 keV peak from thermal noise.

The curve fitting program calculated a standard error for each parameter, using the statistical techniques for multiparameter analysis, and these standard errors were then used to estimate the error in quantities derived from the fitted Mössbauer data. The error in each parameter is a function of the signal to noise ratio of the data and the deviation of the experimental lineshape from a Lorentzian curve, which is caused by crystal field effects and finite absorber thickness[17,41]. The abosrbers used in all experiments contained enriched Fe^{57}, in the chemical form sodium ferrocyanide, in a lucite disk matrix, with iron content of 0.1 to 1.00 mg/cm^2. In most runs the 1.00 or 0.75 mg/cm^2 absorbers were used for maximum percentage effect, since the broadening caused by these absorbers was within acceptable limits. In the experiments concerned with the preparation of a narrow single line source, however, the 0.1 and 0.25 mg/cm^2 absorbers were used so that the linewidth would be closer to natural linewidth.

The geometry of the experimental setup of the spectrometer also needs to be considered in error analysis. On the crank spectrometer an attempt was made to center the absorber between the source and detector to minimize an irrelevant intensity fluctuation caused by varying electronic scattering, due to varying solid angle subtended between the source and absorber and the absorber and detector . This effect was completely negligible in the measurements described in this thesis. Another correction resulting from non-ideal geometry was considered in some cases, and the analysis of this effect is derived in Appendix A. This effect is a result of the fact that the gamma rays passing through the absorber are not strictly parallel, and this effect increases as the distance between source and detector decreases.

B. Mössbauer Spectra for NiO Samples

The temperature dependence of the Mössbauer spectra for a sample of NiO* prepared at 300°C in vacuum is shown in Fig. 7. The spectra can readily be identified as due to Fe^{3+} ions from the isomer shift[42] (approximately -0.4 mm/sec relative to $Na_4Fe(CN)_6 \cdot 10\ H_2O$) and from the hyperfine splitting of the pattern at 81°K, indicating a magnetic field at the nuclear site of order 500 kG[43,44]. At 81°K the pattern is a simple six-line magnetic hyperfine spectrum, but as the temperature was raised a broad unresolved line appeared and gradually became a single line as the six-line pattern disappeared. The collapse of the six-line pattern is gradual, and a narrow single line is reached by 376°K. This is in contrast to a sample of NiO(I) which showed a well defined transition from the antiferromagnetic to the paramagnetic

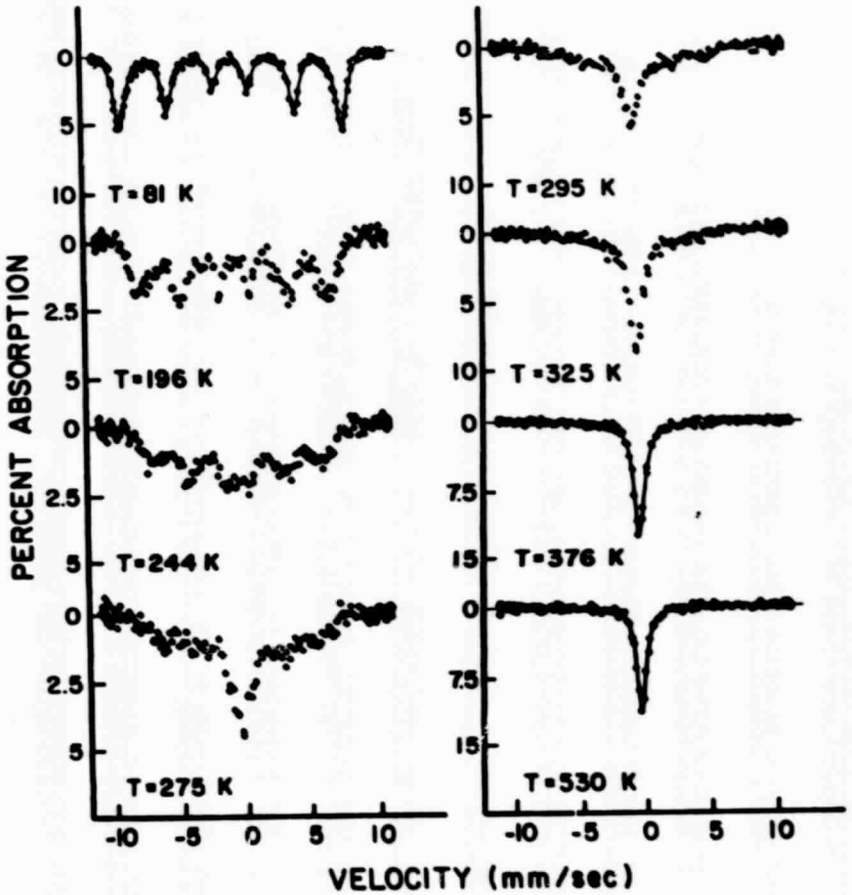

Figure 7. Temperature dependence of Mössbauer spectra for NiO* prepared at 300°C. A 1.00 mg/cm^2 sodium ferrocyanide absorber was used.

state at 525°K. The x-ray particle size indicated for this type of preparation is of order 100 Å, and the density measured with a liquid is about 25% below the theoretical value. Fig. 8 shows the temperature dependence of the Mössbauer spectra for a nominally stoichiometric sample of NiO(II) prepared at 400°C in argon, and again the isomer shift and width of the patterns identify the spectra as due to only the Fe^{3+} ion[42-44]. As the temperature is raised, there is no emergence of the broad unresolved line as in the NiO* samples prepared at 300°C. The higher temperature of preparation appeared to have annealed out the broad component, but the patterns do collapse to a single line below the Néel temperature of defect free NiO(I). A slightly broadened single line is present at 507°K, and the line reaches minimum width by 519°K. The Néel temperature was estimated to be 515 ± 5°K. Fig. 9 shows the temperature dependence of the magnetic field at the nuclear site as determined from the Mössbauer spectra for the sample of NiO(II). The broadened lines were found to be almost purely magnetic, and their broadening is interpreted as being due to a quadrupole interaction with a random electric field gradient, which would arise from the random defect structure proposed for NiO(II). The low temperature limit of the magnetic hyperfine field approaches 550 kG, and this field is characteristic of the Fe^{3+} ion in compounds as compared with values of the order of 200 kG[45] for Fe^{2+}. The temperature dependence of the magnetic hyperfine field at the nucleus was found empirically to follow the Brillouin function for S = 5/2, approximately.

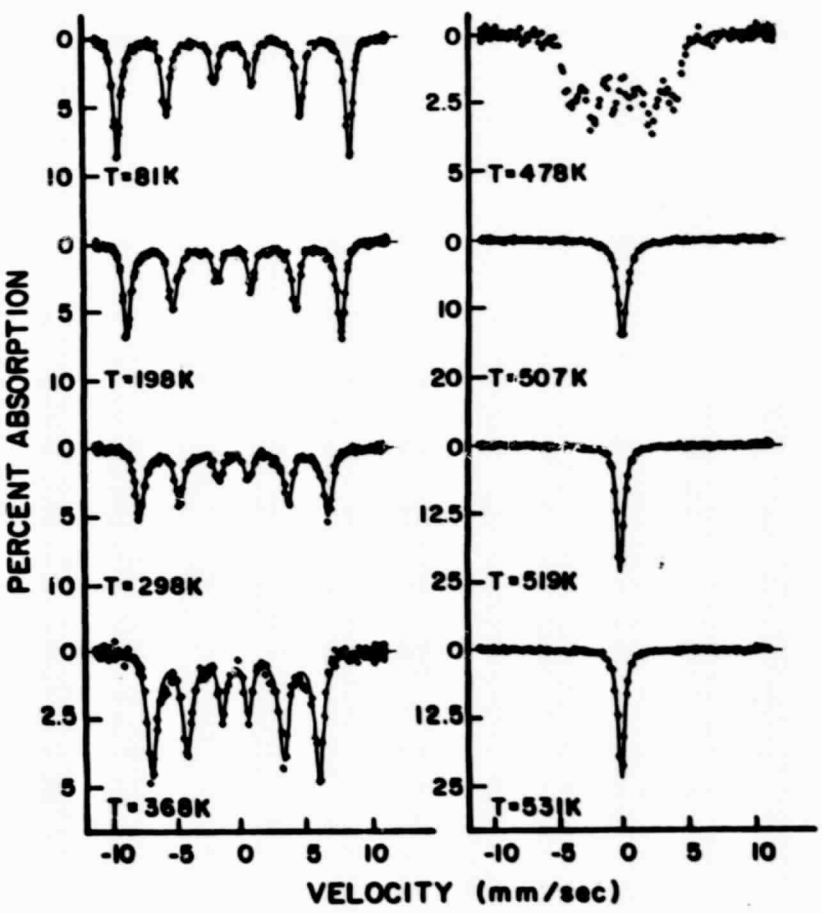

Figure 8. Temperature dependence of Mössbauer spectra for NiO(II) prepared at 400°C. A 1.0 mg/cm² sodium ferrocyanide absorber was used.

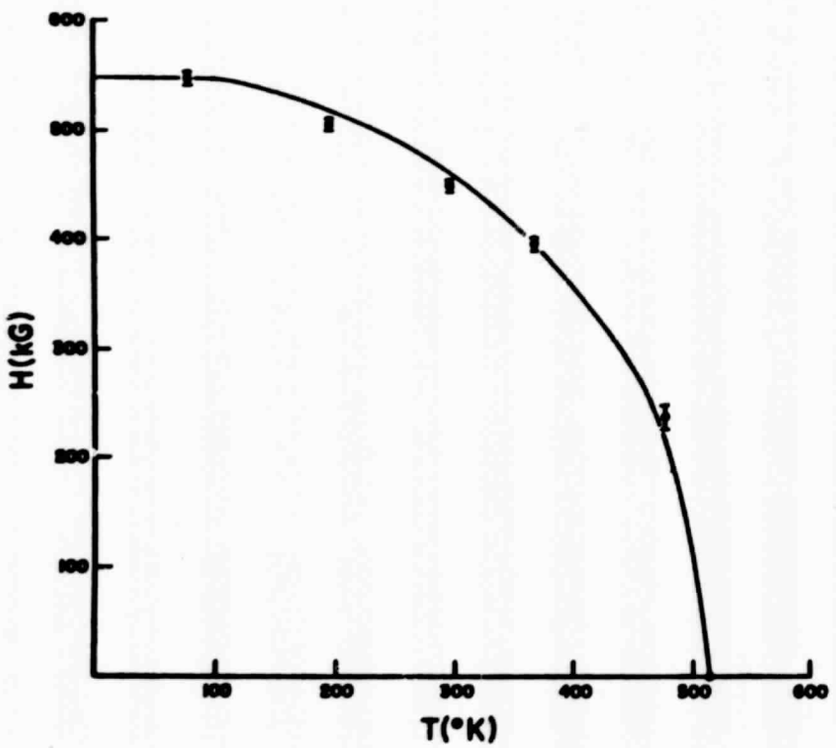

Figure 9. Temperature dependence of magnetic hyperfine field at Fe^{57} site in NiO(II) prepared at 400°C. The solid curve shows the Brillouin function for S = 5/2 .

C. Mössbauer Spectra for Doped Samples

Interesting effects have been observed when CoO and NiO are doped with cations of 1+ and 3+ valence. Significant changes in the ratio of Fe^{2+} to Fe^{3+} resonance have been observed, and these results have added a new dimension to the interpretation of the Mössbauer spectra of these oxides. Fig. 10 shows the effect of adding Li^{1+} to nickelous oxide samples prepared at 800°C in air. The spectra were initially complex with both Fe^{2+} and Fe^{3+} patterns in the Mössbauer resonances, but as the concentration of lithium was increased the ratio of Fe^{3+}/Fe^{2+} increased until only the Fe^{3+} resonance remained. Within experimental error, the line positions of the Fe^{3+} resonances are the same for doped and undoped samples, but the linewidths are narrower for the Fe^{3+} resonance produced in lithium doped samples in high temperature preparations as compared with the Fe^{3+} resonance in NiO(II). Fig. 11 shows the effect of adding Cr^{3+} to NiO(I,II) prepared at 800°C in air. A reduction in the Fe^{3+}/Fe^{2+} ratio was observed at 298°K, while the ratio remained approximately the same at 81°K. Fig. 12 shows similar results for CoO(I,II) prepared at 1000°C in air, where adding Li^{1+} caused the Fe^{3+}/Fe^{2+} ratio to increase at both 81°K and 298°K. Adding Ga^{3+} caused the ratio Fe^{3+}/Fe^{2+} to decrease slightly at 298°K, while the pattern was essentially unchanged at 81°K. Fig. 13 shows the Mössbauer spectra over a range of temperature for a sample of NiO prepared at 1000°C in air with a 1% Li^{1+} doping, which was high enough to completely suppress the Fe^{2+} resonance at all temperatures shown. Again the line positions are the same within experimental errors as for the Fe^{3+} resonance in

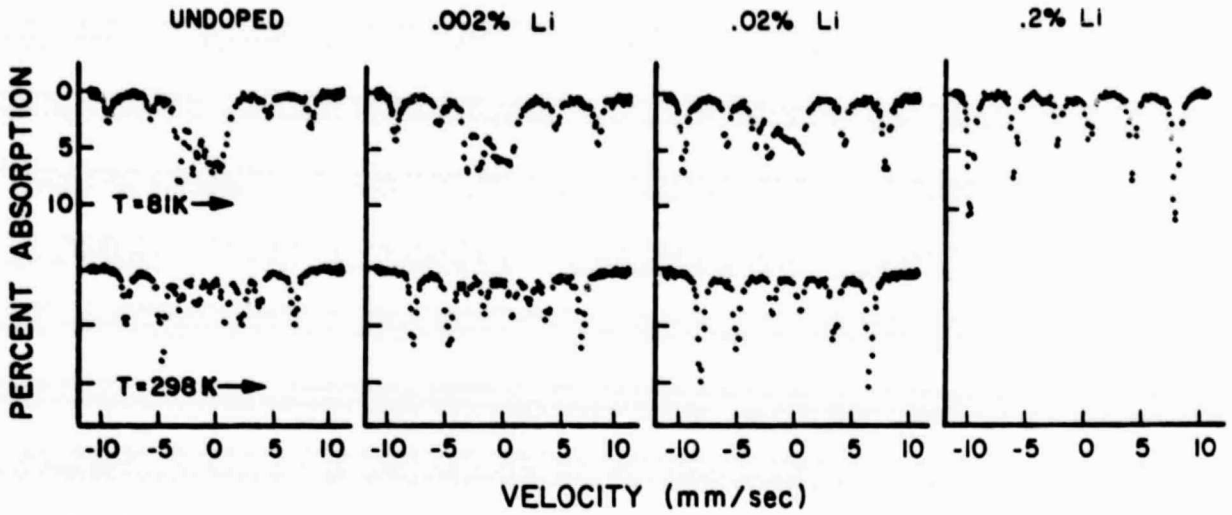

Figure 10. Effect of substitutionally doping with Li^{1+} on the Mössbauer spectra of NiO(I,II) prepared at 800°C. A 1.0 mg/cm^2 sodium ferrocyanide absorber was used.

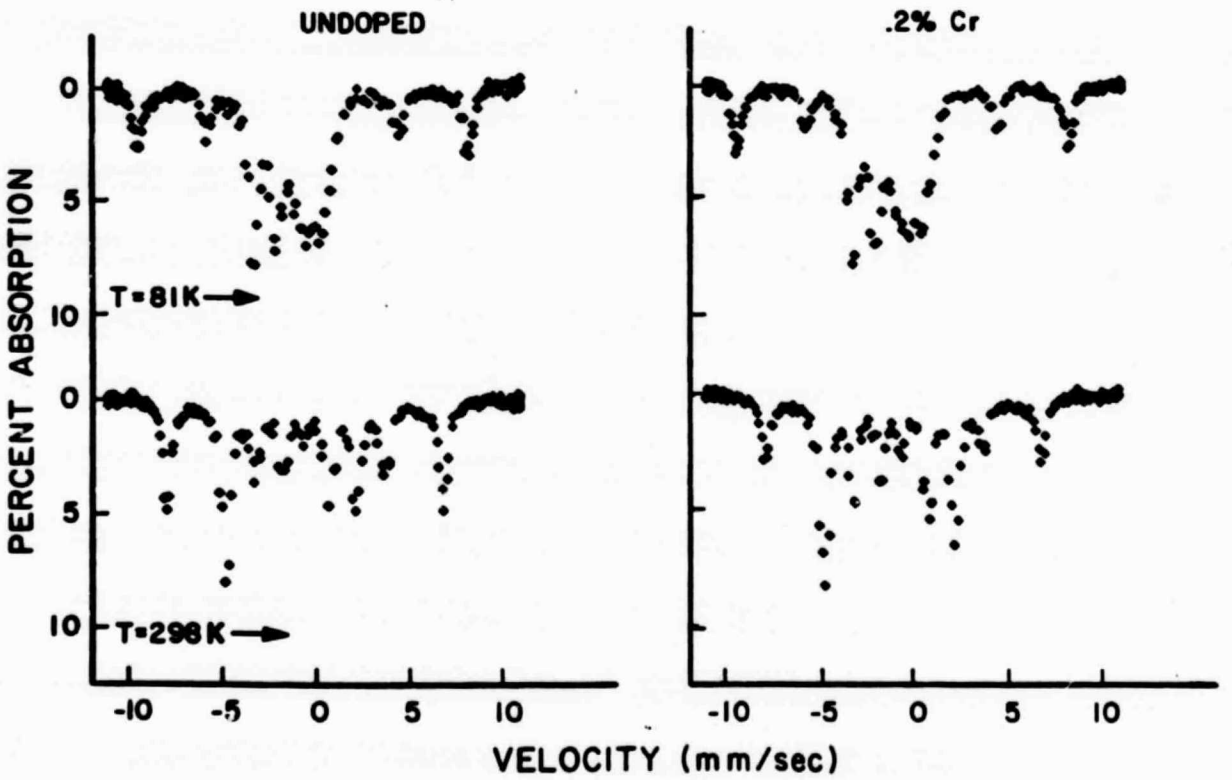

Figure 11. Effect of substitutionally doping with Cr^{3+} on the Mössbauer spectra of NiO(I,II) prepared at 800°C. A 1.0 mg/cm^2 sodium ferrocyanide absorber was used.

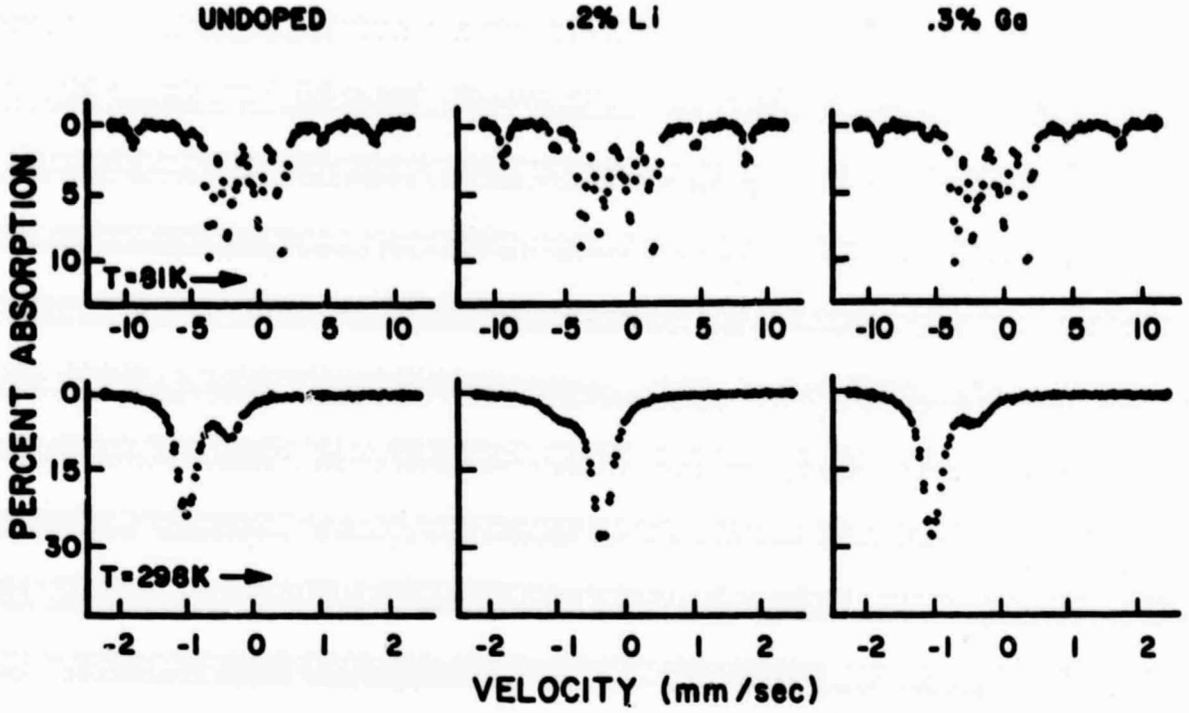

Figure 12. Effect of substitutionally doping with Li^{1+} and Ga^{3+} on the Mössbauer spectra of CoO(I,II) prepared at 1000°C. A 1.0 mg/cm^2 sodium ferrocyanide absorber was used at 81°K and a 0.5 mg/cm^2 absorber at 298°K.

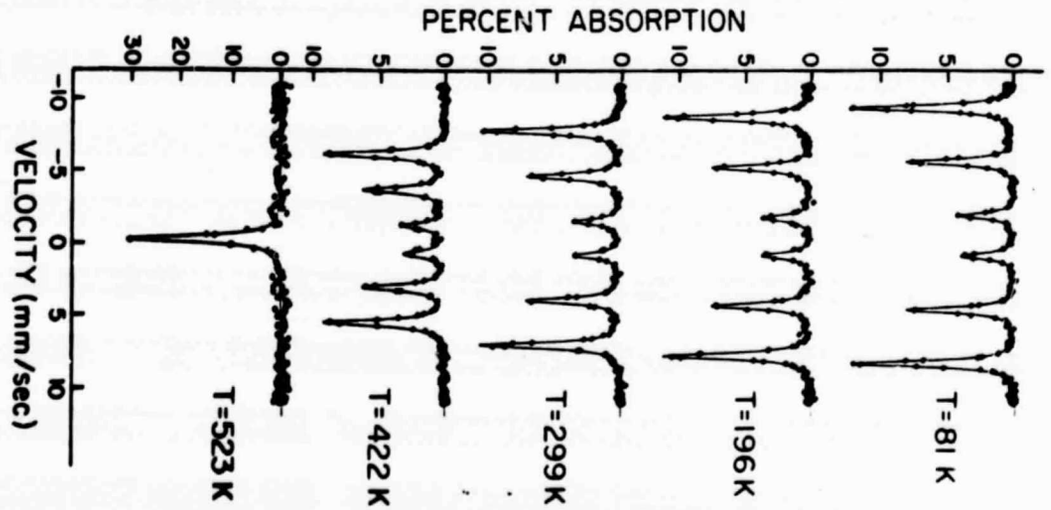

Figure 13. Temperature dependence of Mössbauer spectra for NiO prepared at 1000°C with a 1% Li^{1+} doping. A 1.0 mg/cm^2 sodium ferrocyanide absorber was used.

NiO(II), but the linewidths are narrower by about .2 mm/sec on the average when measured with the same absorber. A similar result was obtained for a sample of CoO prepared at 1000°C in air with a 1% doping of Li^{1+}, and the use of such a sample at room temperature as a hot single-line source is discussed in Section V-H. Figs. 14 and 15 show, respectively, a comparison of the temperature dependence of the Mössbauer spectra for CoO(I,II) and CoO(I,II) with a .1% doping of Li^{1+}. In order to curve fit this data it was necessary to make certain assumptions to reduce the number of parameters because the spectra below the Néel temperature consisted of twelve lines (not counting two small lines resulting from mixing of m states) from the Fe^{2+} and Fe^{3+} resonances. The intensities of the six lines of each resonance were assumed to be in the ratio 3:2:1:1:2:3, and this assumption was made in the curve fitting analysis so that a single area parameter was associated with each six-line curve. Also it has been found that for Fe^{57} in a pure magnetic field, the ratio of the differences in position between the six lines is approximately 1:1:3/4:1:1, and using this assumption the line positions could be specified by two parameters, the position of one line and an incrementing parameter. This approximation could not be made, however, for the Fe^{2+} resonance below about 200°K because of the quadrupole interaction which shifted the line positions such that the differences in velocity were no longer in the ratio expected for a pure magnetic interaction. The Fe^{2+} resonance thus required six line position parameters below 200°K. Also, the assumption that each spectrum contained six lines of equal width was made in fitting the data. These assumptions kept the number

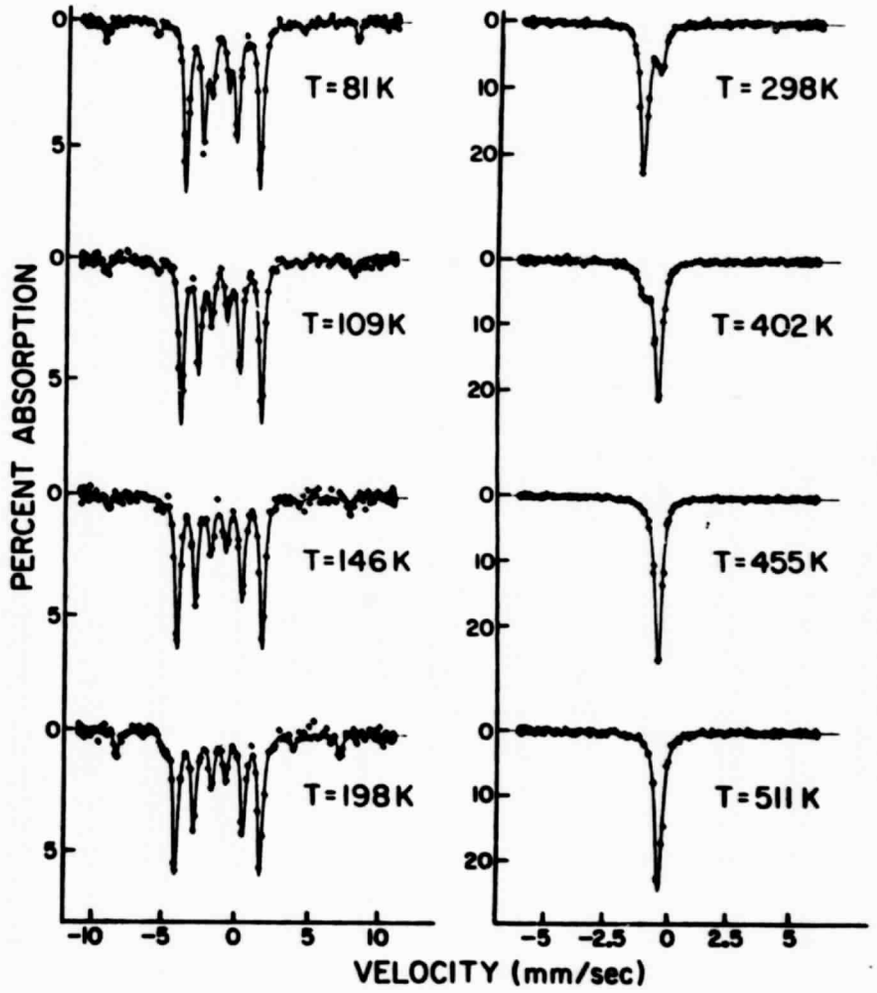

Figure 14. Temperature dependence of Mössbauer spectra for CoO(I,II). A 0.75 mg/cm^2 sodium ferrocyanide absorber was used.

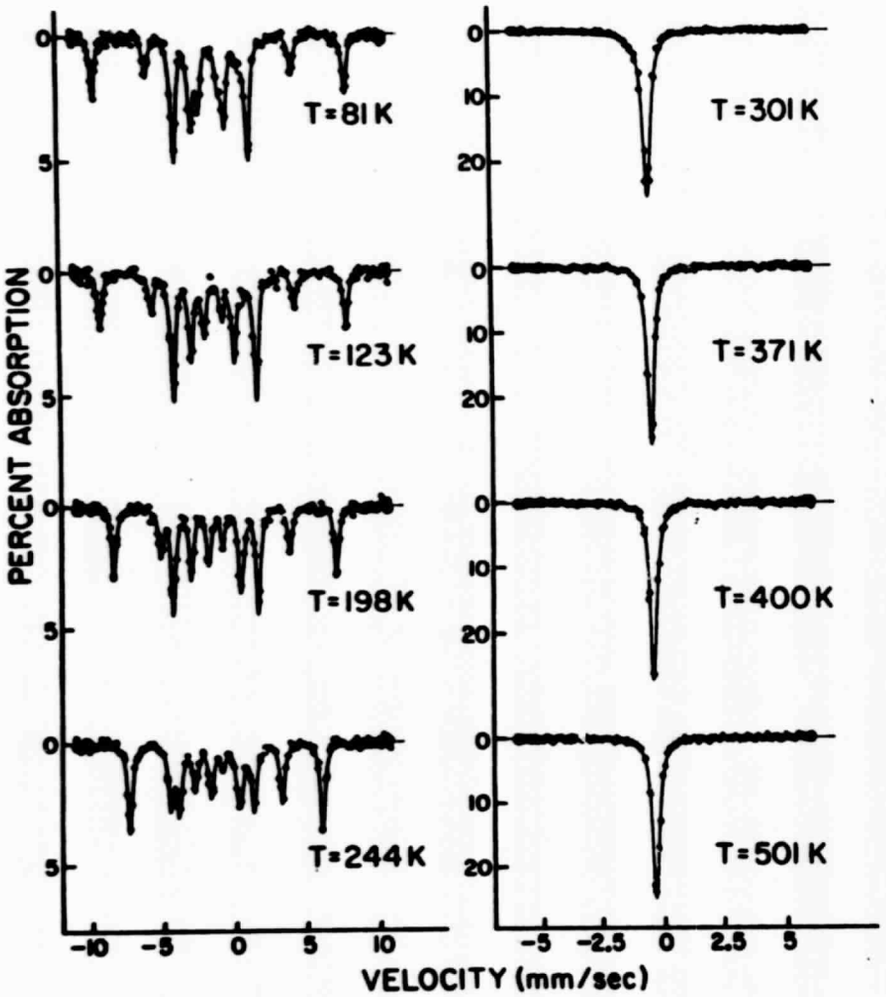

Figure 15. Temperature dependence of Mössbauer spectra for CoO(I,II) with a .1% doping of Li^{1+}. A 0.75 mg/cm^2 sodium ferrocyanide absorber was used.

of parameters within easy management and an excellent fit to the data was obtained. The reason that it was necessary to reduce the number of parameters in this curve fitting was to limit the degrees of freedom to a value consistent with the amount and accuracy of the data points.

D. Temperature Dependence of Recoil-free Fraction

The theory of the recoil-free fraction has already been discussed in Section II-A, where it was shown that the temperature dependence of the area under the Mössbauer curve is related to the binding of ions in the lattice, and may be characterized through the Mössbauer characteristic temperature, θ_m. Fig. 16 shows a plot of the natural logarithm of the area under the curve as a function of T^2 for five different samples, all normalized to the same area at 81°K. The curves represent as follows: (a) the Fe^{3+} resonance in NiO with a 1% Li^{1+} doping, prepared at 1000°C in air, (b) the Fe^{3+} resonance in CoO with a 1% Li^{1+} doping, prepared at 1000°C in air, (c) the Fe^{2+} resonance in CoO(I), (d) the Fe^{3+} resonance in NiO(II), and (e) the Fe^{3+} resonance in CoO(II). The characteristic temperature calculated for each of these cases is, to the nearest 10°K, (a) 420°K for NiO(1% Li), (b) 410°K for CoO(1% Li), (c) 410°K for CoO(I), (d) 350°K for NiO(II), and (e) 230°K for CoO(II). Some of the values are not in exact accord with earlier values reported by MO[11], which is the result of their making the low temperature approximation in calculating θ_m. The present values do not make this approximation and should therefore be more accurate. The significance of the curves is that the Mössbauer characteristic temperature, θ_m, is significantly higher for the Fe^{3+}

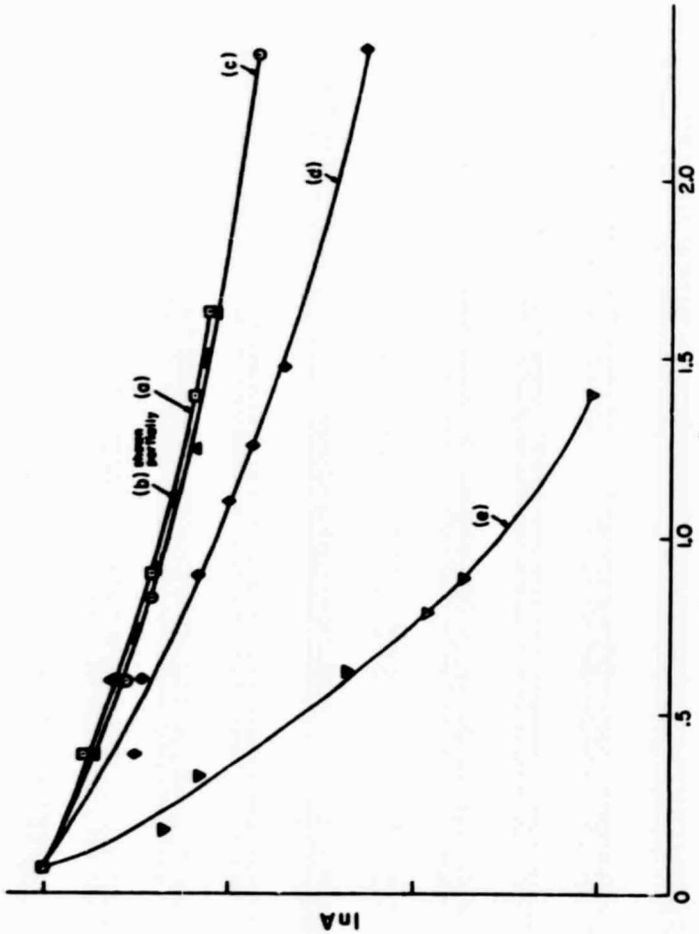

Figure 16. Temperature dependence of ln A for, (a) Fe^{3+} in NiO(1% Li), (b) Fe^{3+} in CoO(1% Li), (c) Fe^{2+} in CoO(I), (d) Fe^{3+} in NiO(II), (e) Fe^{3+} in CoO(II), based on area measurements normalized to unity at 81°K. The first three samples were prepared at 1000°C and the last two at 300-400°C.

resonance induced by Li^{1+} doping in the high temperature preparations, (a) and (b), than for the Fe^{3+} resonance in CoO(II) and NiO(II), (d) and (e). The Fe^{3+} resonance induced by Li^{1+} in high temperature samples has a Mössbauer characteristic temperature which is essentially the same as that of the Fe^{2+} resonance in CoO(I), (c). This strikingly demonstrates the structural differences between the high and low temperature forms of these oxides and rules out merely ion-size or electronic effects as the cause of these differences. This will be discussed in detail in Section VI.

Fig. 17 shows the plot of the natural logarithm of the area under the curve for the Fe^{3+} resonance in CoO(I,II) and CoO(I,II) with a .1% doping of Li^{1+}. The initial value of ln A is higher for the Fe^{3+} resonance in the second sample because of the lithium doping. The curves have different turning points, but they show basically the same type of dependence of area with temperature. Both curves show the unusual increase of area of the Fe^{3+} resonance with temperature which has been observed in these oxides.[4,5,11] The present results appear to permit a simpler explanation of the increase of the area of the Fe^{3+} resonance in CoO(I,II) than the original suggestion[11] that this effect might be the result of the dispersal of anion vacancies above 200°K. This effect now appears to be best understood in terms of the semiconducting properties associated with these materials and will be discussed further in Section VI.

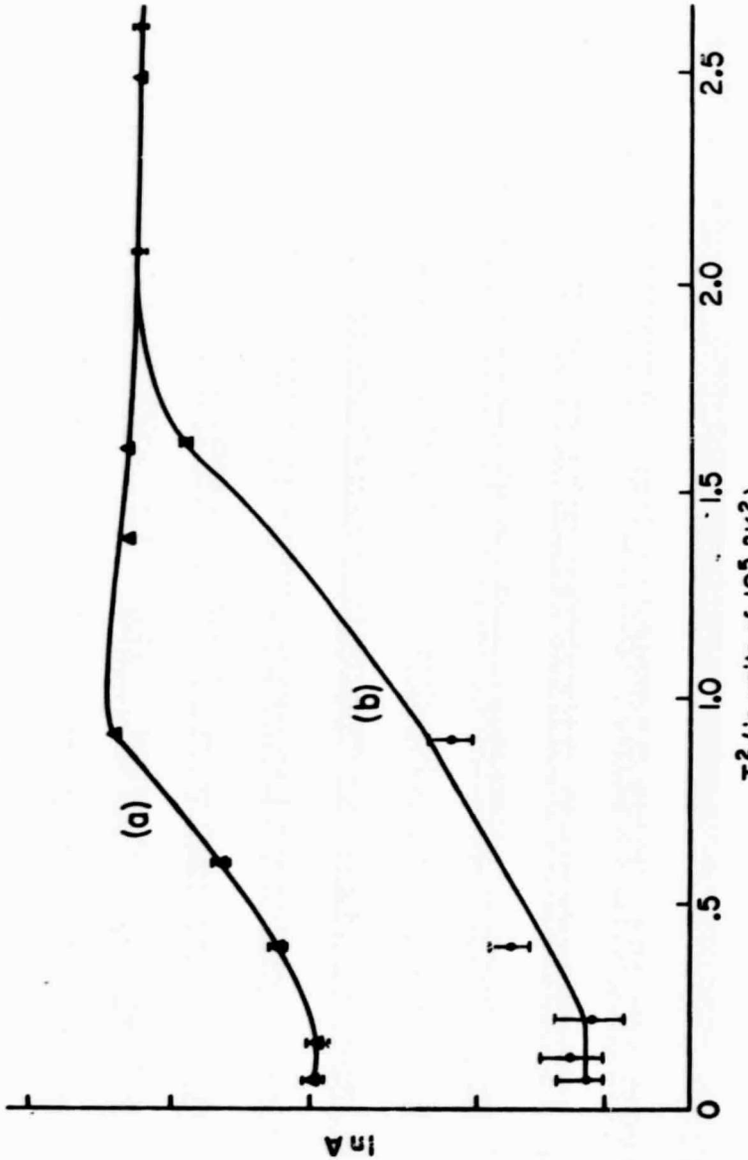

Figure 17. Temperature dependence of ln A for Fe^{3+} in (a) CoO(I,II) with a .1% Li^{1+} doping and (b) CoO(I,II).

E. Néel Temperature

As shown in Section V-B, the Néel temperature for a nominally stoichiometric sample of NiO(II) prepared at 400°C was measured to be 515 ± 5°K. We determined the Néel temperatures of undoped and Li^{1+} doped samples prepared at high temperatures in order to compare with the result for NiO(II). The procedure employed for determining the Néel temperature was to make comparative Mössbauer runs on the sample in increments of approximately 1°K over the temperature range in which the six-line antiferromagnetic pattern changed to a single paramagnetic line. When an undoped high temperature sample of NiO was run in this manner, the Néel temperature was determined to be 525.5 ± 1°K, which may be compared with the values 524 ± 1°K and 525 ± 1°K listed elsewhere[10,46]. The Néel transition was sharp, taking place within a range of about 2°K. A sample of NiO prepared in an identical manner at high temperature except for a 0.9% doping of Li^{1+} was then run in the same manner. Identical geometry was used, which made it possible to determine any Néel temperature difference accurately, regardless of an estimated 1°K possible error in the absolute temperature. A similar sharp transition from the antiferromagnetic to the paramagnetic state was also observed, but corresponding changes in the pattern occurred an average of 4.3°K lower in temperature, which indicated a Néel temperature lowering of about 0.8%, for a Li^{1+} doping of 0.9%. A sample of CoO prepared at high temperature containing 1.1% Li was also run, and the Néel temperature was found to be 284.5°K, which, represents a 1.2% lowering from the Néel temperature of 288°K measured

for CoO(I) by MO[11]. The percentage Néel temperature lowering for high temperature samples is therefore nearly equal to the percent of lithium added, and the plausibility of this result has been discussed in Section II-D. These observations of the character of the Néel temperature lowering permit an estimate of the relative fraction of volume associated with Schottky defects, as compared with porosity in the low density samples of CoO(II) and II), which will be discussed in Section VI.

F. Search for Superparamagnetism and Particle Size Effects

The application of an external magnetic field and the constriction of particle size with the silica gel technique were done in order to look for and study small particle or microcrystal effects. Fig. 18 shows the effect of an external magnetic field of order 50 kG on two samples. Part (a) shows the Mössbauer spectrum of a sample of NiO* prepared by a very short anneal at 300°C in vacuum, which shows a combination of a partially resolved six-line spectrum and a broad single line at 282°K. Upon the application of an external magnetic field of 51.5 kG, a significant amount of the broad single line was converted into the partially resolved six-line spectrum, as is seen in Fig. 18(b). The Mössbauer pattern of this sample at 282°K (well below the Néel temperature) and the change in the pattern upon the application of an external magnetic field are indicative of superparamagnetism resulting from small particle size, as discussed in Section II-C. Part (c) of Fig. 18 shows a sample of NiO prepared at 600°C in air in a matrix of silica gel average diameter 140 Å, whose Mössbauer pattern at 289°K

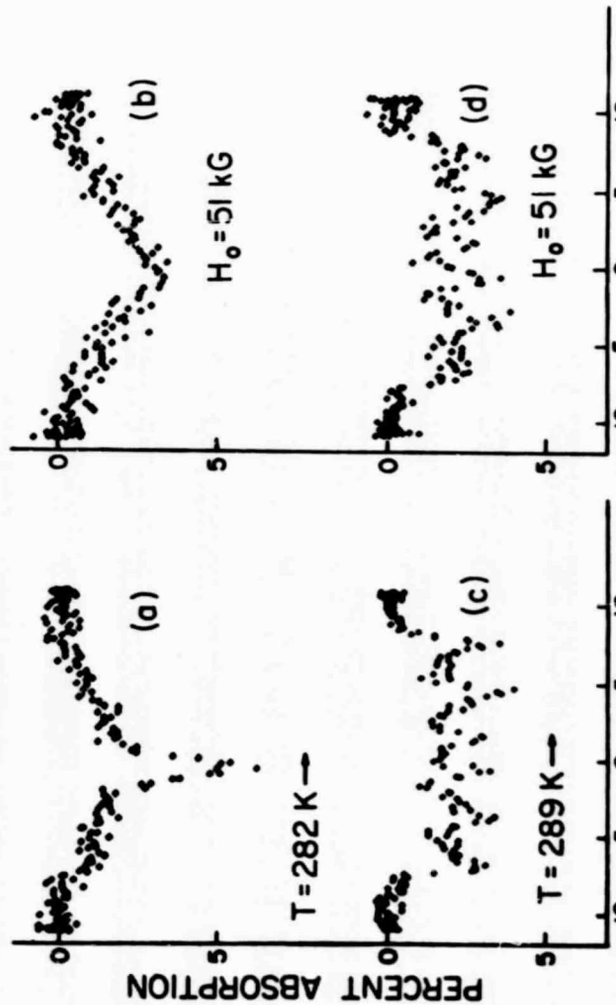

Figure 18. Effect of a 51 kG external magnetic field on the Mössbauer spectra of NiO* prepared by a very short anneal at 300°C, (a) and (b), and on a sample of NiO prepared at 600°C in 140 Å silica gel, (c) and (d).

before the application of the external magnetic field contained a six-line spectrum and a broad unresolved line. The restriction of particle size resulted in a broad unresolved line in addition to the six-line pattern and also gave a pattern resulting from only the Fe^{3+} resonance as measured by the isomer shift. In contrast, an anneal at 600°C in air for a bulk sample produced a NiO(I,II) sample exhibiting both Fe^{2+} and Fe^{3+} resonance with no broad unresolved line. The application of an external magnetic field (d) caused no significant change in the Mössbauer pattern in that the broad unresolved line was not converted into a more resolved spectrum. These two experiments will be discussed further in Section VI, and the results will be correlated with the earlier results obtained by MD[14] upon applying an external magnetic field to CoO(II).

G. Absorber Experiments

Two absorbers of NiO doped with enriched Fe^{57} were made in addition to source experiments. The first absorber was prepared at 300°C in vacuum with a 3% Fe^{57} doping, and its resonance against a Co^{57} in Pd source is shown in Fig. 19 (a). The pattern is complex, containing part six-line spectrum and part doublet pattern, and the separation of the two outer peaks of the six-line pattern is greater than that of the six-line Fe^{3+} resonance in a NiO source at the same temperature. Comparison of the pattern with patterns which have been obtained for Fe^{57} in FeO and Fe_2O_3 absorbers[44, 47, 48] suggests that the Fe^{57} has precipitated out into Fe_2O_3 and FeO inclusions in this preparation. This is not unreasonable because of the high level of Fe^{57} doping

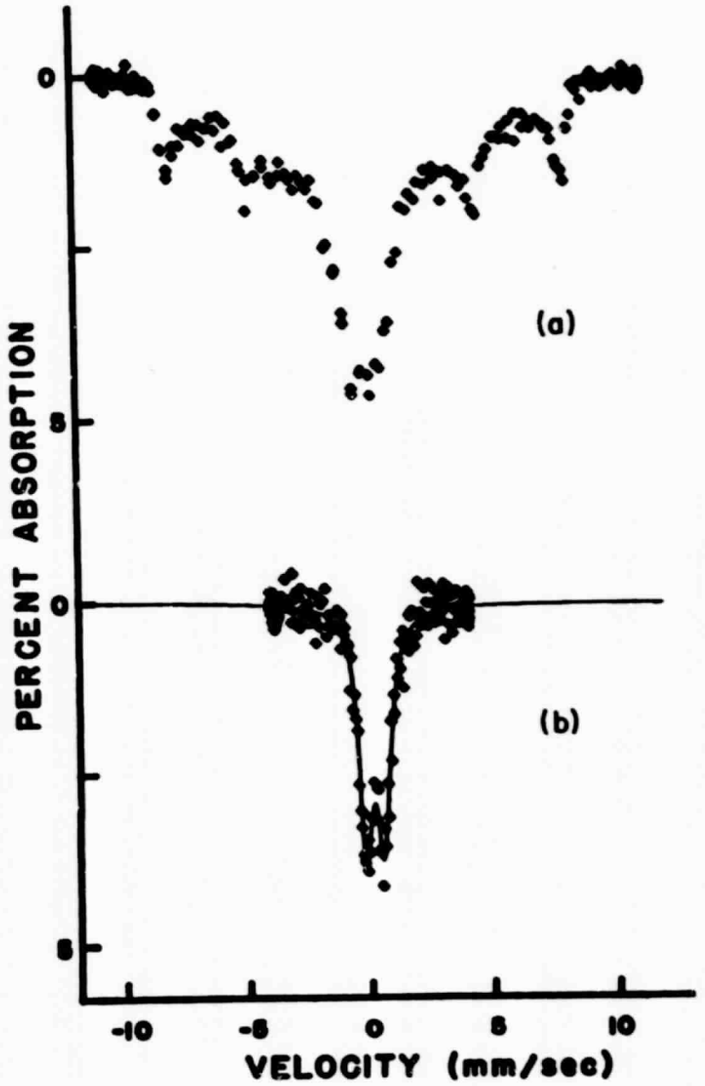

Figure 19. Two absorber resonances, at room temperature, of Fe^{57} in NiO prepared at 300°C. A Co^{57} in Pd source was used.

required in absorber experiments. A second absorber was prepared at 300°C with a 2% Fe^{57} doping, and in this case the initial solution of the nitrates of Fe^{57} and Ni was sprayed into liquid nitrogen with an atomizer in order to freeze the solution very rapidly. The frozen solution was then sublimed before annealing by pumping on the sample with a diffusion pump vacuum while keeping the sample at ice temperature. This technique has been used in experiments with ferrites in an attempt to overcome the problem of inhomogeneous precipitation in a solution containing significant amounts of two different cations. The Mössbauer pattern of this absorber against a Co^{57} in Pd source is shown in Fig. 19(b), and again the pattern is much different from that which would be obtained from a NiO source prepared at the same temperature. The pattern appears to be the same doublet obtained in the first absorber and is similar to the doublet obtained in FeO absorber experiments. It appears, therefore, that the precipitation of Fe^{57} into inclusions of FeO and Fe_2O_3 precludes the possibility of observing the Fe^{3+} source resonance of low temperature oxide preparations in absorbers.

The observation of relaxation effects associated with the emission of Auger electrons by Cavanagh[49] and others[50], motivated an attempt to carry out an experiment on CoO(I,II) with a simultaneous Co^{57} and Fe^{57} doping. The sample was prepared under a CO_2 atmosphere at 1000°C, but with conditions such that a small Fe^{3+} resonance was expected in the source experiment. The Mössbauer results are shown in Fig. 20. While the sample showed the expected resonance pattern, (a), when used as a source, it showed a substantially different pattern when used as an

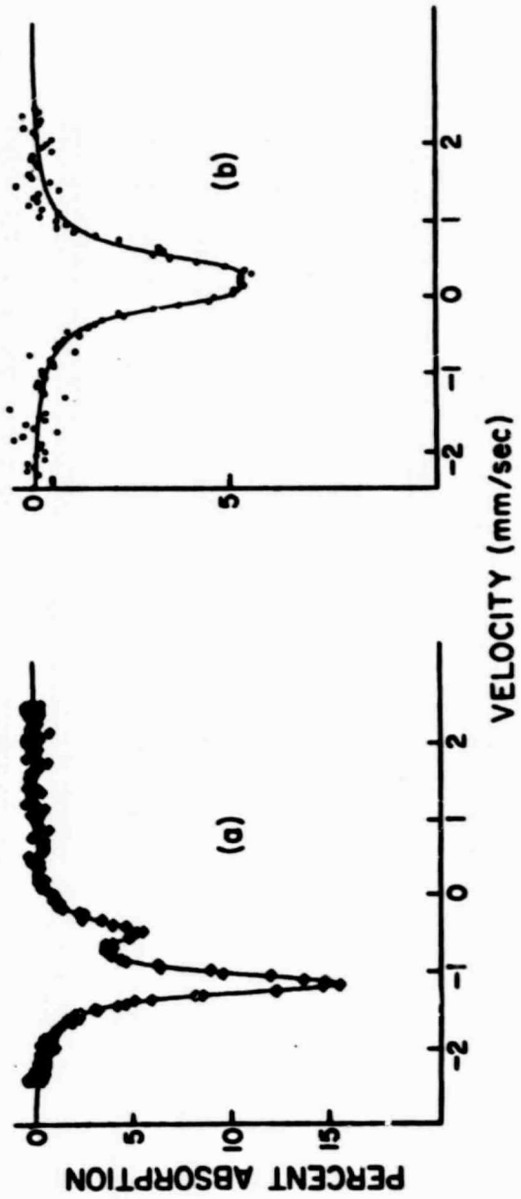

Figure 20. Simultaneous source and absorber Mössbauer spectra, at room temperature, for CoO prepared at 1000°C in CO_2. The source resonance, (a), was run with a 0.25 mg/cm^2 sodium ferrocyanide absorber, and the absorber resonance, (b), with a Co57 in Cu source.

absorber, (b), and the results seem to indicate a precipitation of iron oxide inclusions. This result is at variance with the earlier MO result[11] showing symmetry between the source and absorber, when a very similar preparation technique was used, giving only Fe^{2+} for both the source and absorber experiments. The explanation of these results seems to be that an aging effect, due to a delay in performing the absorber experiment, took place in the sample which resulted in the iron oxide inclusions. Thus, we were not able to determine whether the small amount of Fe^{3+} resonance observed for the source would also have been seen in the absorber.

H. Single-Line Sources

One of the useful tools in Mössbauer spectroscopy is a narrow, room temperature single-line source, and we have found that our doping technique can be useful in the preparation of such sources from CoO. One of the primary motivations for making a source from CoO is that the radioactive Co^{57} is not an impurity. Before the work on cobalt oxide the most common sources were made by diffusing Co^{57} into copper or palladium metal, which gave negligible line broadening and an absence of hyperfine interactions at the nucleus. However, the amount of Co^{57} that can be added to palladium or copper is limited because the quantity of Co^{57} must be kept low enough to avoid broadening from interactions between Co^{57} impurities. One way of reducing this impurity concentration is to diffuse the Co^{57} deeper into the metal, but then the source intensity is reduced because of electronic absorption of the gamma rays. If the source is a compound

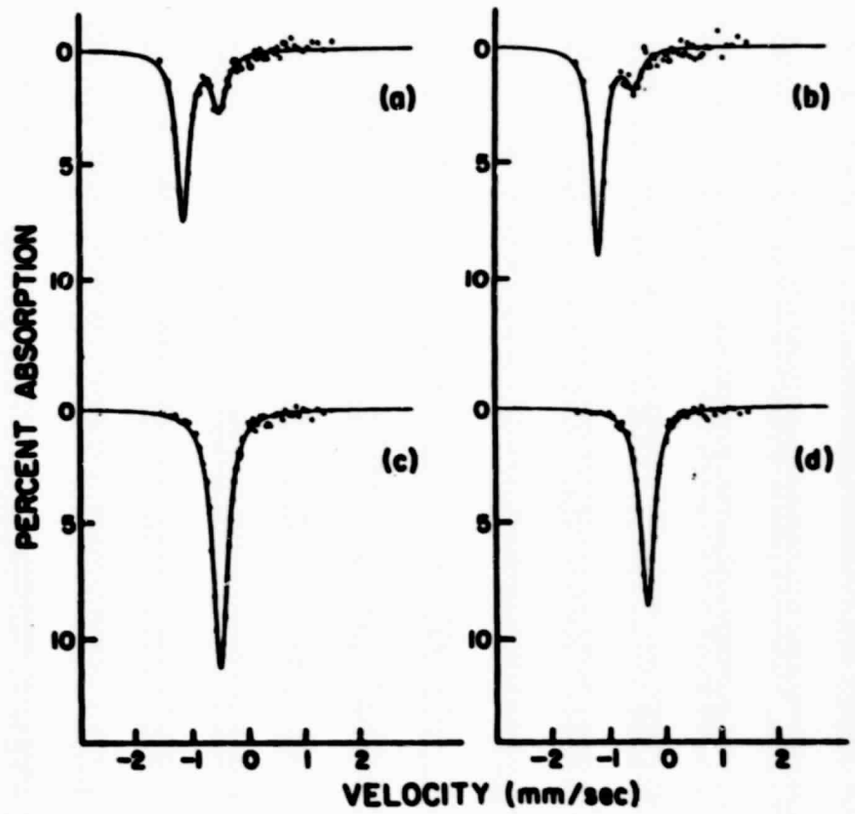

Figure 21. Effects of dopants on Mössbauer spectra at room temperature of CoO, (a) CoO(i,II), (b) CoO(.3% Ga), (c) CoO (1% Li). All of the samples were prepared at 1000°C. (d) an unsplit Pd source. A 0.1 mg/cm^2 sodium ferrocyanide absorber was used in these experiments.

of cobalt, however, the first of these problems does not occur and the second is minimized. MO[51] have discussed the use of the Fe^{2+} resonance of CoO(I) as a hot single-line source, and Stampfel and Flinn[52] have shown that this Fe^{2+} source can be used to make a simple polarized source. However, the preparation of CoO(I) without any Fe^{3+} contamination is difficult in that a successful preparation depends somewhat on the geometry and details of the annealing tube and on the gas flow arrangement. Thus, a certain amount of technique and experimentation are required to prepare pure CoO(I). Fig. 21(a) shows a sample of CoO(I,II) annealed in air at 1000°C, revealing a dominant Fe^{2+} resonance with about 20% Fe^{3+} at room temperature. The same preparation except for the addition of .3% Ga^{3+} and 1% Li^{1+} is shown in parts (b) and (c). In the first case the Fe^{2+} resonance is enhanced, and in the latter case it is completely suppressed. The Ga^{3+} doping should be useful in reducing the possibility of Fe^{3+} contamination when making a CoO(I) source, and the 1% Li^{1+} doping allows the making of a CoO source having only the Fe^{3+} resonance. This latter preparation appears to be insensitive to the exact annealing geometry or other experimental parameters. In contrast to CoO(I), single line sources of CoO(Li) which have not been prepared with adequate care can still be used in many cases because of the suppression of the Fe^{2+} line with increasing temperature. Thus, a small Fe^{2+} component can be eliminated by slightly heating the source above room temperature. When the CoO(1% Li) source is compared with a Co^{57} in Pd source, shown in Fig. 21(d), it is found that the linewidth is only slightly broader (0.02 mm/sec) and the recoil-free fraction is substantially greater.

VI. DISCUSSION

The Mössbauer effect has added a powerful tool for probing the complexities of materials such as the transition metal oxides. Studies of this type have led to considerable debate about the properties of cobaltous oxide and nickelous oxide prepared at low temperatures. Considering all the data taken thus far on these systems, the structural model which seems most compatible with experiment involves a combination of point defects, or vacancies, and small pores. We will show how this picture can explain all of our present results, except for the large oxygen pickup of CoO(II). This latter phenomenon is very striking, and we have no satisfactory explanation for it, thus far. The results indicate that the CoO(II) and NiO(II) samples definitely have significant structural differences from high temperature samples, because the differences between the high and low temperature forms cannot be explained by ion size or electronic effects. The low temperature preparations, stoichiometric CoO(II) and NiO(II), may be viewed as a sponge-like structure formed from sintered microcyrstals, with a large concentration of dispersed point vacancies. The main features of the original MO model[11] are still indicated, in that point vacancies of both cation and anion appear to be the primary cause for most of the observed differences between high and low temperature preparations of these oxides. The data are consistent with the mechanism of charge stabilization for the Fe^{3+} ion proposed earlier, i.e., electron trapping

by oxygen vacancies, analogous to F centers in the alkali halides. (Centers of this type have been observed and studied in MgO.[53]) While our data indicate that small stoichiometric variations may be possible in CoO(II) and NiO(II), these do not appear to be the main cause of their differences.

The general aspects of the Mössbauer spectra, as well as x-ray and chemical data, for NiO samples were found to be similar to those obtained by MO[11] for CoO, indicating that the basic explanations for the properties of these two oxides are the same. We found that a nominally stoichiometric form of NiO, labelled NiO(II), showing only the Fe^{3+} Mössbauer resonance could be prepared at low temperature. NiO(II) represents a saturated non-equilibrium density of Schottky defects and porosity, as in CoO(II). Attempts to increase the density of defects resulted in a non-stoichiometric material, labelled NiO*, with nitrate contamination from the starting material of nickel nitrate, analogous to CoO*. We found that the Fe^{3+} resonance in NiO(II) samples also had a lower Mössbauer characteristic temperature, θ_m, than in high temperature preparations. The x-ray diffraction patterns for NiO(II) samples showed only the expected lines, although broadened. Other similarities, to CoO(II), such as density reduction, were observed for NiO(II). One important difference between CoO(II) and NiO(II) samples is the property of oxygen pickup. In contrast to CoO(II), which was found to pickup more than 60% excess oxygen, NiO(II) was found to be inert when placed in an oxygen atmosphere.

The results of measurements of the pickup of Ar and Ne gas by CoO(II) and NiO(II), discussed in Section IV-D, show that these low

temperature forms physically adsorb a significant amount of these gases. These measurements show that NiO(II) and CoO(II) have a large surface area, and the measurements give an estimate of a particle size of order 100 Å, which is consistent with the x-ray peak broadening shown in Fig. 5 of Section IV-C. In contrast to the physical adsorption of Ar and Ne by CoO(II) and NiO(II), the pickup of oxygen in the early stages by CoO(II), discussed in Section IV-D, can be considered as either a chemical adsorption or some process in which the oxygen diffuses into the lattice, since the oxygen could not be removed by evacuating with a diffusion pump system. We also correlated the oxygen pickup of CoO(II) with x-ray diffraction patterns and Mössbauer spectra, as discussed in Section IV-C. The results are suggestive of a two stage process, but we have not been able to propose a satisfactory explanation which will account for the enormous oxygen pickup and which is, at the same time, consistent with other data, such as the small decrease in the Néel temperature for CoO(II) and the apparent continuous conversion of the Mössbauer pattern from a six line pattern to a two line pattern. Whatever the mechanism of oxygen pickup, we have concluded from the rest of our data that a large surface area and an appreciable quantity of Schottky defects are required. This dramatic pickup of oxygen appears to be too great to be explained by either a simple surface adsorption or an absorption into anion vacancies. Also, a surface adsorption cannot easily account for the continuous transformation of the Mössbauer pattern with the amount of oxygen increase. Thus, further investigation will be required to understand this phenomenon.

The application of an external magnetic field, shown in Fig. 18(a) and (b) of Section V-F, to a sample of NiO* prepared by a very short anneal at 300°C caused some of the broad single line to be converted into a partially resolved six-line spectrum, indicative of superparamagnetism of small particles. The application of an external magnetic field to a second sample of NiO prepared in a matrix of 140 Å silica gel did not result in a significant change in the Mössbauer pattern, as shown in Fig. 18(c) and (d). This latter result seems to indicate that the particles of average diameter 140 Å are too large for superparamagnetic effects to be observed with an external magnetic field of order 50 kG. This can be understood in terms of the discussion in Section II-C, where we indicated the strong dependence of the superparamagnetic relaxation time on particle size. It is also possible that we obtained an alteration in the relaxation time due to the surface of the silica gel. MO[14] found that the application of an external magnetic field to CoO(II) did not give any effect indicative of superparamagnetism. The observation of a change in spin relaxation time for NiO* and a failure to see such a change in CoO(II) may indicate that non-stoichiometric and impure materials such as NiO* and CoO* do indeed possess a microcrystal structure, of a type suggested by Schroeer and Triftshauser.[12] Their model is not adequate to understand the pure and nominally stoichiometric materials, which we have designated as CoO(II) and NiO(II), although the evidence for porosity may indicate a sintered material whose initial components were of a microcrystalline form.

The measured Néel temperature lowering in NiO(II) and CoO(II), as compared with high temperature samples, permits a first order estimate of the relative volume associated with Schottky defects as compared with porosity in these low temperature preparations. Our results, discussed in Section V-E, indicated that the Néel temperature in high temperature lithium doped samples is reduced from the value found for undoped samples by a percentage nearly equal to that percentage of lithium which is substitutionally doped into the lattice for Co or Ni ions (at the level of 1% doping). The plausibility of this result was discussed in Section II-D, where we concluded that the Néel temperature was proportional to the number of second neighbor cations. It was also pointed out that Co or Ni vacancies would be expected to have the same effect as lithium substitutional impurities provided the number of these point defects is small compared to the number of cobalt or nickel ions. This condition is not rigorously satisfied, especially in CoO(II), but this procedure does allow an estimate of the relative partitioning of point vacancies and pores in CoO(II) and NiO(II). The observation of a 6% reduction in T_N for CoO(II) by MO[11] would therefore indicate that about 1/4 of the 25% reduction in density observed for CoO(II) is due to Schottky defects or point vacancies and about 3/4 is due to porosity. As discussed in Section V-B, a sample of NiO(II) had a Néel temperature 2% less than a high temperature form. A similar analysis, therefore, indicates that about 1/6 of the 12% reduction in density observed for NiO(II) is due to point vacancies and 5/6 is due to porosity.

Our data on the temperature dependence of the recoil-free fraction, which may be expressed as a Mössbauer characteristic temperature, θ_m, strikingly demonstrate the structural differences between the high and low temperature forms of these oxides, as presented in Section V-D and shown in Fig. 16. Since the Fe^{3+} ion is smaller than the Fe^{2+} ion, the lower θ_m of the Fe^{3+} resonance in CoO(II) and NiO(II) as opposed to that of Fe^{2+} in high temperature preparations might be explained on the basis of ion size effects. Table 4 contains a summary of ion size data for ions considered in this study (also listed are ion sizes for the three dopants which have been added to NiO and CoO samples, and it can be seen that these ions should fit substitutionally into the cavities of the Co^{2+} or Ni^{2+} ions). If the impurity ion is smaller than the ion it substitutionally replaces it may have a large mean square displacement,[54] which would cause a lower θ_m. This effect will tend to be offset by the tendency of the extra charge of the Fe^{3+} to draw the oxygen ions closer, thereby reducing $\langle u^2 \rangle$. If ion size or charge effects of this type are dominant, we should see the same θ_m for Fe^{3+} in low temperature forms and for the Fe^{3+} resonance induced in high temperature preparations by lithium. In fact, θ_m for Fe^{3+} in high temperature preparations is essentially the same as for Fe^{2+} in high temperature preparations, and is significantly higher than for Fe^{3+} in low temperature preparations. Thus, a comparison of θ_m for CoO(1% Li) and CoO(I) shows no evidence for ion size effects within experimental error, in that the Fe^{2+} and Fe^{3+} resonances in high temperature samples have the same θ_m. Schroeer and Triftshauser attempted to explain the lower value found for θ_m in CoO(II) or

Table 4

Compilation of ion sizes. Values listed are in Å.

Fe^{2+}	Fe^{3+}	Co^{2+}	Ni^{2+}	Li^{1+}	Cr^{3+}	Ga^{3+}
.76 a)	.64 a)	.74 a)	.72 b)	.68 c)	.69 b)	.60 c)
.76 b)	.64 b)	.74 b)	.68 c)	.60 c)	.55 c)	.62 c)
.76 c)	.53 c)	.70 c)	.69 c)	.78 d)	.64 d)	.62 d)
.75 c)	--	.72 c)	.78 d)	--	--	--
.76	.60	.73	.72	.69	.63	.61

a) See reference 8

b) See reference 54

c) See reference 55

d) See reference 58

NiO(II) by a microcrystal model, assuming modifications of the lattice vibrational spectrum. MO[13] showed, using an analysis by Rich[56], however, that this effect is much smaller than required to account for the observed lowering of θ_m. The data are best explained on the basis of Schottky defects, which would reduce the average binding of the Fe^{3+} ion in CoO(II) or NiO(II). It is noteworthy that the fractional reduction in θ_m from high temperature forms for CoO(II) is about 3 times that of NiO(II) and the density of Schottky defects estimated for these materials from the Néel temperature lowering is in the ratio 3:1, which supports the idea that Schottky defects cause the lowering of θ_m.

The data on the temperature dependence of the recoil-free fraction for Fe^{3+} in CoO(I,II) and in CoO(I,II) doped with .1% Li^{1+} give an indication of the reason for the increase of the Fe^{3+} resonance with temperature in CoO(I,II) and NiO(I,II). Bhide and Shenoy[4,5] explained this behavior in terms of a monotonic increase with temperature of the relaxation time for Fe^{3+} going to Fe^{2+}, resulting from a decrease in the capture cross section for the Fe^{3+} ion to obtain electrons. Their overall analysis involved assumptions about Auger aftereffects which were subsequently shown to be wrong.[7,8] Triftshauser and Craig[7,8] attempted to explain the increase of the Fe^{3+} resonance as due to increased mobility of the cation vacancies which they proposed to stabilize the Fe^{3+} resonance. Data on the magnitude of cation diffusion in CoO by Peterson[57] rules out this explanation. MO[11] explained this increase of Fe^{3+} resonance as due to a dispersal of anion vacancies out from simple clusters of CoO(II) in CoO(I,II),

which they also invoked to account for the large oxygen pickup of CoO(II). As discussed in Section V-D and shown in Fig. 17, the increases of the Fe^{3+} resonance with temperature in CoO(I,II) and CoO(I,II) with a .1% lithium doping are qualitatively similar. It is unlikely that the results for the Li^{1+} doped sample can involve a diffusion of lithium in the same temperature region as anion vacancies. These new results obtained with the lithium dopant, therefore, indicate that the increase of the Fe^{3+} resonance with temperature is caused by a shifting of the statistical equilibrium for the ratio of Fe^{2+}/Fe^{3+}. Thus, this effect is a consequence of the semiconducting properties of these materials.

Since CoO and NiO are II-VI compounds we may expect that their electronic behavior will lie somewhere in between the ionic behavior of I-VII compounds and the covalent behavior of III-V compounds. In ionic compounds there is a complete transfer of electronic charge, and in purely covalent compounds there is a sharing of electrons. The effects of the Li^{1+}, Cr^{3+}, and Ga^{3+} dopants, presented in Section V-C, can be explained by a band model for these semiconducting oxides. Other investigators have found that lithium acts as an acceptor, increasing the conductivity significantly, and gallium or chromium act as donors, decreasing the conductivity.[27,29,58-61] Regarding Fe^{2+} as a donor, we obtain a conversion from 2+ to 3+ upon substitutionally inserting an acceptor such as lithium, as shown in Figures 10, 12, 13, 15, and 21. This is based on the assumption that the lithium level lies lower in the band gap than the iron level. The equilibrium ratio Fe^{2+}/Fe^{3+} goes in the opposite direction when donors such as chromium

or gallium are added, as shown in Figures 11, 12, and 21. This is based on the assumption that the chromium and gallium levels lie higher in the band gap than the iron level. A monotonic dependence of the ratio of Fe^{2+}/Fe^{3+} upon the concentration of the dopant was found, as illustrated in Figure 10. Our results indicate that Mössbauer measurements on these oxides might be a useful tool for studying their semiconducting properties, and optical measurements of impurity and band levels in these materials should permit a quantitative comparison with our Mössbauer data. Our doping technique has also proved very useful in the preparation of compact, single line sources from CoO, as discussed in Section V-H and shown in Fig. 21.

LIST OF REFERENCES

LIST OF REFERENCES

1. R. L. Mössbauer, Z. Phvsik 151, 124 (1958).
2. G. K. Wertheim, Phys. Letters 30A, 237 (1969).
3. G. K. Wertheim, Phys. Rev. 124, 764 (1961).
4. V. G. Bhide and G. K. Shenoy, Phys. Rev. 143, 309 (1966).
5. V. G. Bhide and G. K. Shenoy, Phys. Rev. 147, 306 (1966).
6. J. G. Mullen and H. N. Ok, Phys. Rev. Letters 17, 287 (1966).
7. W. Triftshauser and P. P. Craig, Phys. Rev. Letters 16, 1161 (1966).
8. W. Triftshauser and P. P. Craig, Phys. Rev. 162, 274 (1967).
9. K. J. Ando et. al., J. Phys. Chem. Solids 28, 2291 (1967).
10. J. D. Siegwarth, Phys. Rev. 155, 285 (1967).
11. H. N. Ok and J. G. Mullen, Phys. Rev. 168, 550 (1968); 168, 563 (1968); 181, 986(E) (1969).
12. D. Schroeer and W. Triftshauser, Phys. Rev. Letters 20, 1242 (1968).
13. H. N. Ok and J. G. Mullen, Phys. Rev. Letters 21, 823 (1968).
14. H. N. Ok, W. R. Helms, and J. G. Mullen, Phys. Rev. 187, 704 (1969).
15. G. K. Wertheim and D. N. E. Buchanan, Chem. Phys. Letters 3, 87 (1969).
16. H. Frauenfelder, The Mössbauer Effect (W. A. Benjamin Inc., New York, 1963).
17. S. Margulies and J. R. Ehrman, Nucl. Instr. and Methods 12, 131 (1961).

18. A. H. Muir, K. J. Ando, and H. M. Coogan, Mössbauer Effect Data Index 1958-1965 (Interscience Publishers, New York, 1966).
19. C. P. Bean and J. D. Livingston, J. Appl. Phys. Suppl. 30, 120 (1959).
20. I. S. Jacobs and C. P. Bean, Magnetism, edited by G. T. Rado and H. Suhl (Academic Press Inc., New York, 1963) Vol. III.
21. J. S. Smart, Effective Field Theories of Magnetism (W. B. Saunders Co., Philadelphia, 1966).
22. D. C. Khan and K. A. Erickson, Phys. Rev. 1B, 2243 (1970).
23. J. G. Mullen, Phys. Rev. 131, 1410 (1963).
24. R. C. Knauer and J. G. Mullen, Rev. Sci. Instr. 38, 1624 (1967).
25. N. V. Sidgwick, Chemical Elements and Their Compounds (Clarenden Press, Oxford, 1952). Vol. II.
26. J. W. Mellor, A Comprehensive Treatise on Inorganic and Theoretical Chemistry, (Longmans, Green and Co., 1935). Vols. XIV and XV.
27. E. J. W. Verwey et. al., Philips Res. Rep. 5, 173 (1950).
28. R. R. Heikes and W. D. Johnson, J. Chem. Phys. 26, 582 (1957).
29. S. Koide, J. Phys. Soc. Japan 20, 123 (1965).
30. H. P. Klug and L. E. Alexander, X-ray Diffraction Procedures for Polycrystalline and Amorphous Materials (John Wiley and Sons, Inc., New York, 1954).
31. André Guinier, X-ray Crystallographic Technology (Hilger and Watts Ltd., London, 1952).
32. D. A. Skoog and D. M. West, Fundamentals of Analytical Chemistry (Holt, Rinehart, and Winston, New York, 1963). pp. 356-357.
33. N. C. Tombs and H. P. Rooksby, Nature 165, 442 (1950).
34. H. P. Rooksby, Nature 152, 304 (1943).
35. H. P. Rooksby, Acta Crystallographica 1, 226 (1948).
36. A. H. Compton and S. K. Allison, X-rays in Theory and Experiment (D. Van Nostrand Co., Inc., New York, 1935).
37. X-ray Powder Data File, ASTM Special Technical Publication 48-J, 1960, Index Card 4-0835.

38. Although these measurements are reported for NiO(II) and CoO(II), there was a small deviation from stoichiometry. This difficulty was the result of experimental problems involved in preparing large samples of NiO(II) and CoO(II). We do believe, however, that this difficulty was of no particular significance for these measurements.

39. S. Brunauer, The Adsorption of Gases and Vapors (Princeton University Press, Princeton, N. J., 1945).

40. W. Heitler, Quantum Theory of Radiation (Clarendon Press, Oxford, 1949).

41. J. Heberle, Nucl. Instr. and Methods 8, 90 (1968).

42. S. DeBeneditti, G. Lang, and R. Ingalls, Phys. Rev. Letters 6, 60 (1961).

43. O. C. Kistner and A. W. Sunyar, Phys. Rev. Letters 4, 412 (1960).

44. G. K. Wertheim, J. Appl. Phys. Suppl. 32, 110 (1961).

45. K. Ono and A. Ito, J. Phys. Soc. Japan 19, 899 (1964).

46. Charles Kittel, Introduction to Solid State Physics (John Wiley and Sons, Inc., New York, 1967), p. 483.

47. R. W. Vaughan and H. G. Drickamer, J. Chem. Phys. 47, 1530 (1961).

48. G. Shirane, D. E. Cox, and S. L. Ruby, Phys. Rev. 125, 1158 (1962).

49. J. F. Cavanagh, Phys. Stat. Sol. 36, 657 (1969).

50. P. Jung and W. Triftshauser, Phys. Rev. 175, 512 (1968).

51. J. G. Mullen and H. N. Ok, Mössbauer Effect Methodology, edited by I. J. Gruverman (Plenum Press, New York, 1968), Vol. 4.

52. J. P. Stampfel and P. A. Flinn, Mössbauer Effect Methodology (Plenum Press, New York, 1970), Vol. 6.

53. L. A. Kappers, R. L. Kroes, and E. B. Hensley, Phys. Rev. (to be published).

54. P. Auzins, J. W. Orton, and J. E. Wertz, Paramagnetic Resonance, edited by W. Low (Academic Press, New York, 1963), Vol. I.

55. F. A. Cotton and G. Wilkinson, Advanced Inorganic Chemistry (Interscience Publishers, New York, 1966).

56. M. Rich, Phys. Letters 4, 153 (1963).

57. W. K. Chen, N. L. Peterson, and W. T. Reeves, Phys. Rev. 186, 887 (1969).

58. G. M. Schwab and H. Schmid, J. Appl. Phys. 33S, 426 (1962).

59. I. G. Austin, A. J. Springthorpe, and B. A. Smith, Phys. Letters 21, 20 (1966).

60. A. J. Bosman and C. Crevecoeur, Phys. Rev. 144, 763 (1965).

61. S. Van Houten, J. Phys. Chem. Solids 17, 7 (1960).

APPENDIX A

A GEOMETRICAL EFFECT IN MÖSSBAUER SPECTROSCOPY

In actual Mössbauer experiments the detector samples a range of doppler velocities for any horizontal velocity v of the absorber, which is a geometrical effect arising from perpendicular components of the gamma ray momentum relative to the doppler motion. This is an inevitable consequence of the finite size of the source and detector. The experimental geometry is shown in Fig. 22, where only the effects of detector size are considered. The source is considered as a point source, and the gamma rays make angles of 0 to θ_1 with the horizontal line between the source and center of the detector window. The average doppler velocity may be calculated by averaging over the solid angle subtended by the detector as follows:

$$E_d = \frac{E_\gamma}{c} \langle v \cos\theta \rangle = \frac{E_\gamma}{c} \langle v_x \rangle \quad .$$

The quantity $\langle v_x \rangle / v$ may be calculated as follows:

$$\frac{\langle v_x \rangle}{v} = \frac{\int_0^{\theta_1} (v \cos\theta)\, 2\pi r^2 \sin\theta \, d\theta}{v \int_0^{\theta_1} 2\pi r^2 \sin\theta \, d\theta} \quad ,$$

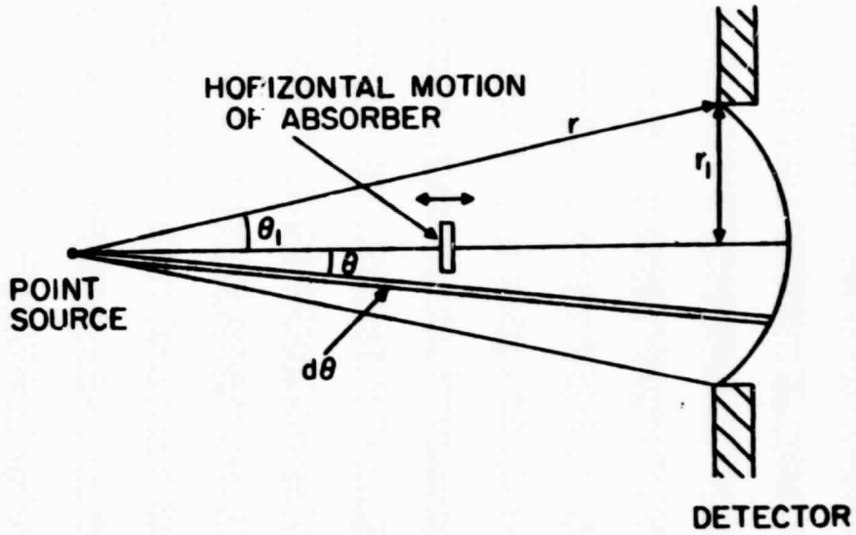

Figure 22. Experimental geometry illustrating the solid angle subtended by the detector of a Mössbauer spectrometer.

which reduces to:

$$\frac{\langle v_x \rangle}{v} = \frac{\int_0^{\theta_1} \cos\theta \sin\theta \, d\theta}{\int_0^{\theta_1} \sin\theta \, d\theta} = \frac{1}{2}(1 + \cos\theta_1) \quad .$$

Since θ_1 will almost certainly be a small angle, the following approximation can be made:

$$\frac{\langle v_x \rangle}{v} = \frac{1}{2}(1 + \cos\theta_1) \cong 1 - \frac{\theta_1^2}{4} \quad .$$

The effective doppler velocity is thus reduced by the factor $\frac{\theta_1^2}{4}$, and to obtain the correct doppler velocity we must multiply the experimental velocity by the factor $(1 - \frac{\theta_1^2}{4})$. Table 5 gives this correction term for various values of $\sin\theta_1 = \frac{r_1}{r}$. The intensity of the Mössbauer absorption lines as a function of any angle θ of the absorber will be:

$$I = \frac{S\Gamma/2\pi}{(v_o - v\cos\theta)^2 + \Gamma^2/4} \quad ,$$

which may be averaged over solid angle to obtain an average intensity as follows:

$$\langle I \rangle = \frac{S\Gamma/2\pi \int_0^{\theta_1} \frac{2\pi r^2 \sin\theta \, d\theta}{(v_o - v\cos\theta)^2 + \Gamma^2/4}}{\int_0^{\theta_1} 2\pi r^2 \sin\theta \, d\theta} \quad ,$$

Table 5

Correction factors for geometrical effect.

$\sin\theta_1 = \frac{r_1}{r}$	$1 - \frac{\theta_1^2}{4}$	% Effect
.05	.9994	.06
.10	.9970	.3
.15	.9940	.6
.20	.9895	1.1
.25	.9850	1.5
.30	.9775	2.3

which partially reduces to:

$$\langle I \rangle = \frac{S\Gamma}{2\pi(1 - \cos\theta_1)} \int_0^{\theta_1} \frac{\sin\theta \, d\theta}{(v_o - v\cos\theta)^2 + \Gamma^2/4}$$

The integration may be performed by a change of variables:

$$\alpha = (v_o - v\cos\theta) \quad ,$$

to yield:

$$\langle I \rangle = \frac{S}{\pi v(1 - \cos\theta_1)} \left[\tan^{-1}\left(\frac{v_o - v\cos\theta_1}{\Gamma/2}\right) - \tan^{-1}\left(\frac{v_o - v}{\Gamma/2}\right) \right]$$

Numerical computer calculations were made in order to calculate the area under the curve using the above expression for $\langle I \rangle$. It was found that the experimental area must be multiplied by the factor, $(1 - \frac{\theta_1^2}{4})$, to obtain the correct area. A look at Table 5 indicates that the correction factor, $(1 - \frac{\theta_1^2}{4})$, will be less than 1% for a separation of 3 inches between source and a one inch diameter detector. However, the correction for this effect may be necessary in experiments involving very careful measurement of lineshape or peak position.